Universitat Ramon Llull

DOCTORAL THESIS

Title	**Development of a new chemical sensor based on plasma polymerized polypyrrole films**
Presented by	**Jose Luis Yagüe Marrón**
Centre	**Escola Tècnica Superior IQS**
Department	**Enginyeria Industrial**
Directed by	**Dr. Salvador Borrós Gómez**

C. Claravall, 1-3
08022 Barcelona
Tel. 936 022 200
Fax 936 022 249
E-mail: urlsc@sec.url.es
www.url.es

A mi abuela

"Un hombre puede hacer lo que quiera,
pero no querer lo que quiera"
Arthur Schopenhauer

AGRADECIMIENTOS

El desarrollo de esta tesis no habría sido posible sin la ayuda de muchas personas con las que me he rodeado durante este periodo tan importante de mi vida. Me siento afortunado por haber tenido su apoyo, colaboración y sobre todo, amistad y cariño.

En primer lugar te quiero dar las gracias a ti Chicho, por toda la confianza que depositaste en mí, por este proyecto que me diste y que ha ido madurando y me ha hecho madurar en estos años y por los nuevos proyectos que han de venir. Por todos los baches, los éxitos, las decepciones y las alegrías, esta tesis también te pertenece.

I would like to thank Dr. Zineb Mekhalif for giving me the opportunity to work in the CES laboratory in Namur, it really helped me to develop my thesis. Thanks to you and also Dr. Joseph Delhalle for all the advices and facilities during my stay. Thanks to everyone in the CES group, especially Jess, Greg, Jorge and Isabelle, for your collaboration, patience and the time we shared, I'll never forget the big fire! (Je vous promets que la prochaine fois je parlerais le français un peu mieux), and to the people working on the 3rd floor for all the crazy moments, it was fan-tas-tic!!! També agrair a l'Anna B, l'Anna C, la Maria i el Toni per venir a veure'm a Namur i animar-me en un moment complicat per a mi.

Thanks to Dr. Karen Gleason for allowing me to characterize my polymer in the Department of Chemical Engineering at MIT. Y también a Laura por ayudarme con todas las técnicas y equipos del laboratorio y por darme un sitio donde dormir en Boston (aunque fuera en el suelo).

Gràcies als Departament d'Orgànica i d'Anàlisis del IQS on es va dur a terme alguns dels experiments d'aquesta tesi i al Centre nacional de Microelectrònica pel desenvolupament de l'elèctrode de 4 puntes. També agrair al IQS per la beca de doctorat atorgada i a la Generalitat de Catalunya per la beca de mobilitat BE-2008.

Quisiera agradecer a toda la gente de GEMAT que he conocido durante todos estos años (que no han sido pocos) por todos esos pequeños momentos de charla, de risas y alguna vez de trabajo, que me han hecho disfrutar tanto de esta época de mi vida y que volvería a repetir sin dudarlo ni un segundo. A Mares per haver cregut en aquest

projecte a l'hora de fer el TFC, i al Víctor per l'ajut en les correccions. Pero agradecer especialmente, por todo el tiempo que hemos compartido, a Berta, Núria, David, Miki y muy especialmente a ti Mariona, por todo lo que me has dado, siempre estarás conmigo.

A Raimon, mi infatigable amigo durante todo el doctorado, por estar aguantándome día sí, día también, espero que aún nos quede mucho más por compartir aunque hayamos acabado ya la tesis y muy especialmente por nuestra tradición de los viernes. A todos los amigos de la promoción, por ser una vía de escape de los problemas y presiones y por todos los grandes momentos que hemos pasado.
A los amigos del colegio, Xavi, Pepe, Pere, Dani, Pitu y Miguel, porque después de veinticinco años de conocernos aún seguimos juntos, ¡que no es fácil! Y me habéis demostrado lo que significa ser un amigo. Y las que se han ido añadiendo poco a poco a nuestro grupo: Berta, Anabel, Laias, i els més petits Claudia, Júlia i l'Adrià.

Sin olvidarme de mi familia, mis tíos y primos por estar siempre ahí aunque no nos podamos ver mucho. A mi abuela Lola por esas súper-comidas familiares los domingos. Y a mis dos abuelos y mi abuela, que ahora no están pero siempre los tenemos presentes. A ti Alex, porque aunque los dos vayamos a la nuestra siempre me tendrás ahí. Y principalmente, a mis padres, por mantener vuestra confianza en mí, por apoyarme en mis proyectos y por aguantarme en mis malos momentos, que siempre acababa pagando con los que más quiero. Por todo esto, espero algún día poder devolveros todo lo que me habéis dado.

SUMMARY

This thesis contributes a new insight into surface modification involving substrates nanostructuration by self-assembly to deposit on them a conducting polymer through plasma enhanced chemical vapor deposition. The use of conducting polymers has gained growing interest in the development of chemical sensor arrays for gas analysis in electronic engineering applications. The size reduction in these devices has encouraged the proposal of an alternative method to achieve structures at nanometer range, as well as overcoming problems like lack of adhesion between substrate and polymer, lower limits of detection or shorten response times.

The investigation has dealt with the use of pyrrole terminated monolayers to enhance the nucleation and growth of polypyrrole plasma polymerized films. In addition, monolayers provide an improvement in the interfacial adhesion of the polymer/metal structure. Furthermore, polymeric thin films have been doped to obtain the conducting form of polypyrrole, of which electric properties enable to use it as a chemical sensor. Exposure to vapors leads to changes in polymer conductivity, by which analytes can be identified and quantified.

Self-assembly and polymer deposition are key factors in this research, as a consequence surface characterization techniques, such as XPS, TOF-SIMS, FT-IR or SEM, have been employed to study their physical and chemical characteristics. Especially interesting have been the use of AFM to investigate the nucleation process and the film topography. Moreover, the four-point probe technique has provided an excellent tool to perform conductivity measurements on thin films. Besides, plasma polymerized films have shown a high sensitivity to carbon dioxide in order to demonstrate their aptitudes to be utilized as a chemical sensor.

RESUMEN

La presente tesis contribuye a dar una nueva visión dentro del área de modificación de superficies, la cual implica la nanoestructuración de sustratos utilizando la técnica de auto-ensamblado para depositar sobre éstos un polímero conductor mediante deposición química en fase vapor por plasma. El uso de polímeros conductores ha despertado un creciente interés en el desarrollo de sensores químicos para el análisis de gases en aplicaciones de ingeniería electrónica. La continua reducción de tamaño en estos dispositivos ha alentado la propuesta de un método alternativo para conseguir estructuras de rango nanométrico, así como para solucionar problemas tales como la falta de adherencia entre sustrato y polímero, disminuir los límites de detección o acortar los tiempos de respuesta.

En esta investigación se ha trabajado con monocapas con un grupo pirrol terminal para potenciar la nucleación y crecimiento de películas de polipirrol polimerizadas mediante plasma. Además, las monocapas han aportado mejoras en la adhesión interfacial de la estructura polímero/metal. Asimismo, se han dopado las películas delgadas de polipirrol para obtener su forma conductora, cuyas propiedades eléctricas permiten utilizarlo como sensor químico. Su exposición a un vapor conlleva cambios en la conductividad del polímero, a través de los cuales se puede identificar y cuantificar dicho analito.

El auto-ensamblaje y la deposición del polímero son los factores claves en esta investigación. Por lo tanto, se han utilizado diversas técnicas de caracterización de superficies, como XPS, TOF-SIMS, FT-IR o SEM, para estudiar sus propiedades físicas y químicas. Igualmente, el uso del AFM ha sido de gran valor para investigar el proceso de nucleación y la topografía de las películas. Además, la técnica de las cuatro puntas ha proporcionado una excelente herramienta para realizar medidas de conductividad en películas delgadas. Finalmente, las películas polimerizadas por plasma han mostrado una gran sensibilidad al dióxido de carbono, con lo cual han demostrado su capacidad para ser utilizados como sensores químicos.

RESUM

La present tesis contribueix a donar una nova visió dins de l'àrea de modificació de superfícies, la qual implica la nanoestructuració de substrats fent servir la tècnica d'auto-assemblatge per a dipositar sobre aquests un polímer conductor mitjançant deposició química en fase vapor per plasma. L'ús de polímers conductors ha despertat un creixent interès en el desenvolupament de sensors químics per a l'anàlisi de gasos en aplicacions d'enginyeria electrònica. La contínua reducció de mida en aquests dispositius ha encoratjat la proposta d'un mètode alternatiu per aconseguir estructures de rang nanomètric, així com per solucionar problemes com la falta d'adherència entre substrat i polímer, disminuir els límits de detecció o escurçar els temps de resposta.

En aquesta investigació s'ha treballat amb monocapes amb un grup pirrol terminal per tal de potenciar la nucleació i creixement de pel·lícules de polipirrol polimeritzades mitjançant plasma. A més, les monocapes han aportat millores en l'adhesió interfacial de l'estructura polímer/metall. Així mateix, s'han dopat les pel·lícules primes de polipirrol per tal d'obtenir la seva forma conductora, les propietats elèctriques de les quals permeten utilitzar-ho com a sensor químic. La seva exposició a un vapor comporta canvis en la conductivitat del polímer, a través dels quals es pot identificar i quantificar l'esmentat analit.

L'auto-assemblatge i la deposició del polímer són els factors claus en aquesta investigació. Per tant, s'han utilitzat diverses tècniques de caracterització de superfícies com XPS, TOF-SIMS, FT-IR o SEM, per estudiar les seves propietats físiques i químiques. Igualment, l'ús de l'AFM ha estat de gran ajut per investigar el procés de nucleació i la topografia de les pel·lícules. A més, la tècnica de les quatre puntes ha proporcionat una excel·lent eina per realitzar mesures de conductivitat a les pel·lícules primes. Finalment, les pel·lícules polimeritzades per plasma han mostrat una gran sensibilitat al diòxid de carboni, demostrant la seva capacitat per ser utilitzades com a sensors químics.

ABBREVIATIONS

2P	two-point probe
4P	four-point probe
AFM	Atomic Force Microscopy
ASTM	American Society for Testing and Materials
BF	Blocking Factor
CF	Correction Factor
CP	Conducting Polymer
CV	Cyclic Voltammetry
DC	Duty Cycle
DNA	Deoxyribonucleic acid
^{1}H-NMR	Proton Nuclear Magnetic Resonance
F_{DESORP}	Desorption flow
FIB	Focused Ion Beam
F_{LEAK}	Leakage Flow
F_{MON}	Monomer Flow
FT-IR	Fourier Transform Infrared
F_{TOT}	Total Flow
HOMO	Highest Occupied Molecular Orbital
IP	Interdigital Probe
IRRAS	Infrared Reflection Absorption Spectroscopy
ITO	Indium Tin Oxide
LUMO	Lowest Unoccupied Molecular Orbital
MCT	Mercury-Cadmium-Telluride
MEMS	Micro-Electro Mechanical System
MOS	Metal Oxide Semiconductor
MOSFET	Metal Oxide Semiconductor Field Effect Transistor
PECVD	Plasma-Enhanced Chemical Vapor Deposition
P_{eq}	Equivalent Power
PM-IRRAS	Polarization Modulation Infrared Reflection Absorption Spectroscopy
P_{peak}	Peak Power
PPy	Polypyrrole
Py3SH	3-(N-pyrrolyl)propanethiol
Py6SeH	6-(N-pyrrolyl)hexaneselenol

Py6SH	6-(N-pyrrolyl)hexanethiol
Py11Si	11-(pyrrol-1-yl-undecyl)dimethylchlorosilane
Py12SeH	12-(N-pyrrolyl)dodecaneselenol
Py12SH	12-(N-pyrrolyl)dodecanethiol
QCM	Quartz Crystal Microbalance
RMS	Root Mean Square
SAM	Self-Assembled Monolayer
SAW	Surface Acoustic Wave
sccm	standard cubic centimetres per minute
SCE	Saturated Calomel Electrode
SEM	Scanning Electron Microscopy
SPR	Surface Plasmon Resonance
SSCE	Siver/Silver chloride electrode
TOF-SIMS	Time Of Flight Secondary Ion Mass Spectrometry
t_{OFF}	plasma OFF time
t_{ON}	plasma ON time
XPS	X-ray Photoelectron Spectroscopy

TABLE OF CONTENTS

CHAPTER 1

INTRODUCTION

1. INTRODUCTION

1.1 MOTIVATION

The multiple functions and potential applications of nanotechnology have turned it into a necessary and powerful tool in the day-to-day scientific work. Nanotechnology is highly interdisciplinary, involving physics, chemistry, biology, materials science and the full range of engineering disciplines. Its versatility has meant a growing use in a wide range of fields. For instance, electronic engineering has shown an increasing interest in the design of micro/nanoelectronic devices due to their continuously miniaturization. Several efforts have been focus on the fabrication of new electronic circuits and their interconnections.[1-10] Additionally, advances in nanoscale particle design provide new options for drug delivery and drug therapies.[11-16] Even on chemical catalysis, nanotechnology plays already an important role in the synthesis of novel materials with tailored features and chemical properties.[17-21] These are only a few examples of possible applications in which nanotechnology is involved.

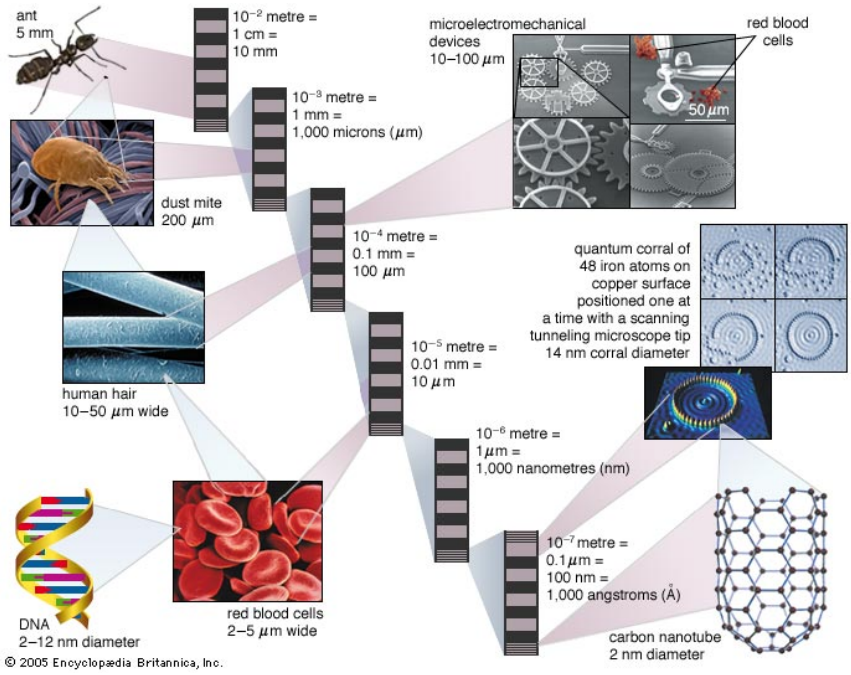

Figure 1. Schematic representation of the reducing size from macroscale to nanoscale.

Besides, to achieve these minute structures there are different kinds of nanofabrication methods which can be divided roughly into two groups: top-down and bottom-up methods. Top-down are based mainly on lithographic patterning techniques using

short-wavelength optical sources. The principle is using specific tools for reducing the substrate into the desired size and shape. Usually, a photoresist (photosensitive coating of an organic polymer) is deposited on the surface of a silicon wafer or a film. Then, a beam of light (UV-light or X-rays) passes through a mask and a lens. The parts exposed to the light can be removed easily leaving the desired pattern. This is the typical nanofabrication method employed in the semiconductor industry. According to Moore's law, the number of transistors places on an integrated circuit doubles every two years. In this sense, further progress in scaling down dimensions is limited by lithography itself. As long as the number of transistors increases, the cost of production to reduce its size increases as well. In addition, other factors, like leakage current or heat dissipation, indicate that it should be convenient to find other ways to create these nanostructures.

In addition, there are the bottom-up methods. In such methods, atoms and molecules organize themselves to create tiny nanostructures. This approach allows controlling shape, size and composition of the nanostructures. Furthermore, it is a very cheap process as it involves only chemical reactions for the synthesis of these materials and it offers the opportunity of using organic components.

Molecular self-assembly is an important aspect of the bottom-up approach to nanotechnology as it uses chemical or physical forces to assemble small units into larger structures. Actually, self-assembly is a common mechanism in nature, where peptides fold to form proteins and enzymes, single-stranded DNA finds its complement and form a double-stranded helix, or phospholipids align themselves in order to form cell walls. These processes are facilitated by specific molecular interactions and the drive to minimize the energy of interaction between molecules. Therefore, humans try to mimic these nature architectures whose natural structures have been taken as a model.

One of these methods is the formation of self-assembled monolayers (SAMs), a single layer of ordered molecules adsorbed spontaneously on a substrate due to the bond between the surface and molecular head groups. SAMs offer a unique combination of physical properties that allow fundamental studies of interfacial chemistry, solvent-molecule interactions and self-organization. Their well-ordered arrays and ease of functionalization make them ideal model systems in many fields. A general system for n-alkyl monolayers can be seen in Figure 2. It consists of an anchoring group bound to a substrate. Depending on the surface, a specific group will be required for that

purpose. Some of the most common examples are based on the interactions between thiols or disulfides and a gold substrate[22-25] or silanes and a silicon wafer.[26-28] The central part of the monolayer is the spacer chain, formed by methylenes which rule the monolayer ordering. Due to Van der Waals interactions between side chains, the monolayer packs tightly and thereby reduces its free energy. Finally, the spacer chain leaves the head group top on the surface. This group rules the chemistry on the surface; this means that it is possible to tailor the interfacial properties of metals, metal oxides and semiconductors by selecting the appropriate functionality.

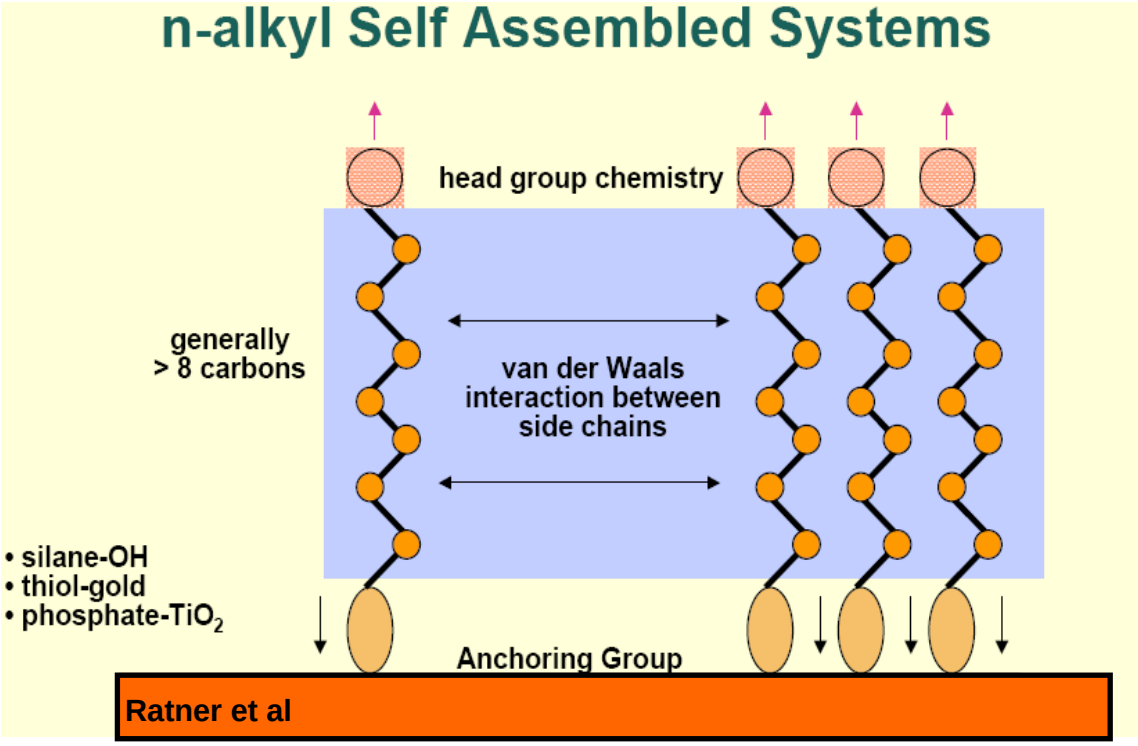

Figure 2. Scheme of a n-alkyl self assembled system according to Ratner *et al.*

Multiple possible applications are available working with the chemistry of the head group. Numerous investigations have been made to tune the wettability of the substrate by the substitution of the terminal group by a hydrophilic or hydrophobic head group.[29-32] Furthermore, SAMs have been used efficiently as corrosion inhibitor.[33-37] Due to the strong bound of the anchoring group to the metal and the compact packing, a homogeneous hydrophobic thin film is formed which serves as a barrier for water, oxygen or electron migration to the metal surface.

Additionally, Simon *et al*[38] in 1981 demonstrated the enhancing effect of monolayers on a polymer deposition process. They proved that N-(3-(trimethoxysilyl)-propyl)pyrrole SAMs, anchored to n-type Si semiconductors via reaction of surface hydroxyl groups,

served as covalently anchoring sites for electrochemically polypyrrole (PPy) deposition. This investigation opened a new insight in the deposition of conducting polymers on SAM-modified substrates. Rubinstein *et al*[39] found later that the assembling of a p-aminothiophenol monolayer on a gold substrate resulted in a substantial increase in film density for electrochemically grown polyaniline films. They attributed this effect to a more efficient nucleation-growth process due to the terminal functional group of the monolayer. Related to this, Willicut and McCarley[40] described in detail the chemistry associated with the assembly of ω-(N-pyrrolyl)alkanethiol monolayers on gold and their effects on the nucleation and growth of polypyrrole films. Similar work was carried out by Wu[41] in which the effect of SAMs structure on charge transport properties was analyzed.

Deposition of conducting polymers is a very interesting topic to work in due to their potential applications. Especially, organic thin films have attracted lot of attention for building electronic devices.[42-44] Mechanical flexibility, low cost or simplified manufacturing are some of the properties which make them promising candidates for micro/nanoelectronic applications.[45-46] Nevertheless, the lack of adhesion between polymer and substrate is one of the problems to deal with. The physics and chemistry of the metal/polymer interface are critical for the overall properties of the device. In this sense, SAMs can act as an adhesion promoter between the two layers to prevent delamination. To overcome the adhesion problem, several studies have been performed based on the affinity of some organic SAMs to the studied surface. Phosphonic acid monolayer has been assembled on engineering metals, such as steel, aluminium, copper and brass, to improve the adhesion with fluoropolymers and ethylene-co-methacrylic acid.[47] Additionally, previous work has revealed that it is possible to assemble conductive films of gold on flexible polymer substrates using silanes with amino- or mercapto-terminal groups.[48] Even on biological assays, it has been shown that functionalized alkanethiols can promote the growth of neurites in electrodes for neural prostheses.[49]

Related to the use of polymers for electronic applications, the development of a chemical gas sensor has received considerable attention in the last decades. In concrete, the fabrication of a chemical sensor array which could be integrated in what is known as an electronic nose. An electronic nose is a device that identifies and quantifies an odour or a combination of different compounds. Electronic noses are another example of biomimetics, human-made devices which imitates nature. An odor is composed of molecules, each of which has a specific size and shape. Each of these

molecules has a correspondingly sized and shaped receptor in the human nose. When a specific receptor receives a molecule, it sends a signal to the brain and the brain identifies the smell associated with that particular molecule. Electronic noses based on the biological model work in a similar manner, albeit substituting sensors for the receptors, and transmitting the signal to a program for processing, rather than to the brain.

When analyzing a sample, the gas is introduced into the device in order to interact with the sensor. This interaction leads to a response signal caused by conductivity variation of the sensor. Then, a pattern recognition algorithm is used on the output signal to classify the odor. It should be noted that odor recognition needs a previous training. Known samples are used as patterns to obtain a response from the chemical sensor array. Each odor has a specific response which is like a fingerprint. Then, patterns are used to create a database which will be used to classify and identify unknown samples.

The electronic device is based on the electrical properties of the sensor. The more commonly used sensors include metal oxide semiconductors (MOS), conducting polymers (CP), quartz crystal microbalance (QCM), surface acoustic wave (SAW) and field effect transistors (MOSFET). The chemical diversity, the sensitivity and the short response time of conducting polymers compare highly favourably to the others sensors. Related to this, the possibility to modify and functionalized the polymer allows tuning the reactivity in front a specific analyte to increase sensitivity.

Among all the possible CP candidates, PPy seems to be an excellent option to work with, because of its mechanical and electric properties.[50] Actually, PPy films have been extensively employed as chemical sensors in a wide range of applications. One of the first attempts to use PPy thin films as the sensor element was carried out by Freund and Lewis.[51] They worked with chemically synthesized PPy films which were plasticized during deposition to provide a systematic control over the chemical binding properties of each sensor. Furthermore, Fang *et al*[52] described the design and fabrication of micro-gas-sensors using electrochemically and chemically oxidised PPy to study ethanol vapour concentration. Additionally, PPy chemiresistors are being employed as humidity sensors due to their high sensitivity to moisture.[53]

As it has been commented before, a typical problem for these sensors is the lack of adhesion between the polymer and the electrode surface, usually a metal. Self-assembly seems to be a very elegant and easy option to solve this problem. Moreover,

a pyrrole-terminated monolayer not only can act as an adhesion promoter but can help the growth of PPy as well. Thereby, the use of SAMs can enhance the deposition of the polymer on the electrode and can prolong its lifetime.

On the other hand, conventional techniques, like chemical oxidation and electrochemistry, have been employed for PPy deposition as usual methods. Since synthesis conditions and physical and chemical properties of these polymerizations have been numerously described, they have become a usual way to obtain polymers. In particular, electrochemistry methods have gained more attention as they enable a higher control in their properties. Even like this, an alternative to these synthetic methods is plasma polymerization.

Plasma polymerization refers to the formation of polymeric materials under the influence of plasma (partially ionized gas). In contrast with conventional techniques, plasma polymerization is a solventless technique which enables the formation of uniform and pinhole free ultra thin films with an absolute control in the deposition rate. In general, plasma polymerization consists of the introduction of the monomer into a reaction chamber in which through plasma activation the monomer reacts to yield the polymer. Because there is no need of aqueous or organic solvents, all the possible contaminations associated in these processes are avoided. Moreover, given that the monomer flow and the experimental conditions, such as power or pressure, can be controlled during the experiment, the growth of nanometer-size films can be achieved. Plasma deposit coatings generally have a complete surface coverage and essentially are made free of voids. Certainly, plasma polymerization is a kind of polymerization itself, what that means is that the product obtained is not the same as in conventional techniques. The differences in polymer formation mechanism and the properties of resultant polymers material process lead to think plasma polymerization as a new method of polymerization.

In general, plasma polymerization seems to be an excellent choice to deposit PPy thin films to be used as chemical sensors due to their electrical properties. As far as SAMs are concerned, no precedent studies have investigated the effect of the monolayer on the nucleation-growth process by plasma-enhanced chemical vapour deposition (PECVD) to our knowledge. The enhancing effect of SAMs on the polymer deposition was demonstrated using a solvent as media with conventional techniques, but no investigations have been reported concerning the deposition from vapour phase.

Because all the exposed, the aim of this thesis is the development of a chemical sensor which is based on plasma polymerized PPy thin films deposited on SAM-modified surfaces. To achieve it, the objectives of the present work are depicted next:

- Formation and characterization of different SAMs with a pyrrole-terminated group on specific surfaces.
- Study of the SAM effect on the nucleation-growth mechanism of polypyrrole on the different substrates by plasma enhanced chemical vapor deposition.
- Synthesis of polypyrrole-like films by plasma polymerization and evaluation of their characteristic features using diverse experimental conditions.
- Doping of the plasma polymerized films to obtain the conductive form of polypyrrole and conductivity measurement of these films.
- Study of different gases by measuring the conductivity change owed to the interaction polymer-analyte in order to perform a qualitative and quantitative analysis.

1.2 THESIS FRAMEWORK

The structure of this thesis has been divided into three chapters according to the different areas of knowledge that it deals with.

The second chapter focuses on the formation of SAMs: the synthesis of target molecules and the processes to perform the self-assembly. The molecules synthesized have always a pyrrole-terminated group but different anchoring groups in order to be assembled on different kind of surfaces. The monolayers have been intensively characterized to determine their quality. The idea in this chapter is the surface nanomodification in order to functionalize the substrate.

In the third chapter, the plasma polymerization process is discussed. Firstly, the SAM effect on the nucleation-growth mechanism has been studied by comparing the PPy deposition on SAM-modified and unmodified substrates. Secondly, the formation of plasma PPy thin films has been analyzed. Finally, the doping process has been carried out and the iodine introduction into the polymer backbone investigated. The purpose of this chapter is synthesizing conducting polymers with proper physical and chemical properties by plasma polymerization.

The fourth chapter provides information about the electrical properties of plasma polymerized PPy thin films. To carry out this aim, it has been necessary to develop a new kind of electrodes and a gas chamber to measure the conductivity. The purpose in this chapter has been to demonstrate the use of these plasma polymerized PPy thin films as chemical sensors for gas analysis.

1.3 REFERENCES

1. Tao, N. J. Electron transport in molecular junctions. *Nature Nanotechnology* **2006,** *1* (3), 173-181.

2. Stan, M. R.; Franzon, P. D.; Goldstein, S. C.; Lach, J. C.; Ziegler, M. M. Molecular electronics: From devices and interconnect to circuits and architecture. *Proceedings of the Ieee* **2003,** *91* (11), 1940-1957.

3. Haselman, M.; Hauck, S. The Future of Integrated Circuits: A Survey of Nanoelectronics. *Proceedings of the Ieee* **2010,** *98* (1), 11-38.

4. Eda, G.; Fanchini, G.; Chhowalla, M. Large-area ultrathin films of reduced graphene oxide as a transparent and flexible electronic material. *Nature Nanotechnology* **2008,** *3* (5), 270-274.

5. Zhang, D. H.; Ryu, K.; Liu, X. L.; Polikarpov, E.; Ly, J.; Tompson, M. E.; Zhou, C. W. Transparent, conductive, and flexible carbon nanotube films and their application in organic light-emitting diodes. *Nano Letters* **2006,** *6* (9), 1880-1886.

6. Kan, S.; Mokari, T.; Rothenberg, E.; Banin, U. Synthesis and size-dependent properties of zinc-blende semiconductor quantum rods. *Nature Materials* **2003,** *2* (3), 155-158.

7. Kumar, S.; Nann, T. Shape control of II-VI semiconductor nanomateriats. *Small* **2006,** *2* (3), 316-329.

8. Chau, R.; Datta, S.; Doczy, M.; Doyle, B.; Jin, J.; Kavalieros, J.; Majumdar, A.; Metz, M.; Radosavljevic, M. Benchmarking nanotechnology for high-performance and low-power logic transistor applications. *Ieee Transactions on Nanotechnology* **2005,** *4* (2), 153-158.

9. Wong, H. S. P. Beyond the conventional transistor. *Ibm Journal of Research and Development* **2002,** *46* (2-3), 133-168.

10. Kovtyukhova, N. I.; Mallouk, T. E. Nanowires as building blocks for self-assembling logic and memory circuits. *Chemistry-A European Journal* **2002,** *8* (19), 4355-4363.

11. Peppas, N. A.; Hilt, J. Z.; Khademhosseini, A.; Langer, R. Hydrogels in biology and medicine: From molecular principles to bionanotechnology. *Advanced Materials* **2006,** *18* (11), 1345-1360.

12. Allen, T. M.; Cullis, P. R. Drug delivery systems: Entering the mainstream. *Science* **2004,** *303* (5665), 1818-1822.

13. Lavan, D. A.; McGuire, T.; Langer, R. Small-scale systems for in vivo drug delivery. *Nature Biotechnology* **2003,** *21* (10), 1184-1191.

14. Panyam, J.; Labhasetwar, V. Biodegradable nanoparticles for drug and gene delivery to cells and tissue. *Advanced Drug Delivery Reviews* **2003,** *55* (3), 329-347.

15. Brigger, I.; Dubernet, C.; Couvreur, P. Nanoparticles in cancer therapy and diagnosis. *Advanced Drug Delivery Reviews* **2002,** *54* (5), 631-651.

16. Rosler, A.; Vandermeulen, G. W. M.; Klok, H. A. Advanced drug delivery devices via self-assembly of amphiphilic block copolymers. *Advanced Drug Delivery Reviews* **2001,** *53* (1), 95-108.

17. Daniel, M. C.; Astruc, D. Gold nanoparticles: Assembly, supramolecular chemistry, quantum-size-related properties, and applications toward biology, catalysis, and nanotechnology. *Chemical Reviews* **2004,** *104* (1), 293-346.

18. Gibbs, J. G.; Zhao, Y. P. Design and Characterization of Rotational Multicomponent Catalytic Nanomotors. *Small* **2009,** *5* (20), 2304-2308.

19. Tian, Z. R. R.; Voigt, J. A.; Liu, J.; McKenzie, B.; McDermott, M. J.; Rodriguez, M. A.; Konishi, H.; Xu, H. F. Complex and oriented ZnO nanostructures. *Nature Materials* **2003,** *2* (12), 821-826.

20. Jia, H. F.; Zhu, G. Y.; Vugrinovich, B.; Kataphinan, W.; Reneker, D. H.; Wang, P. Enzyme-carrying polymeric nanofibers prepared via electrospinning for use as unique biocatalysts. *Biotechnology Progress* **2002,** *18* (5), 1027-1032.

21. Wang, Z. G.; Wilner, O. I.; Willner, I. Self-assembly of aptamer-circular DNA nanostructures for controlled biocatalysis. *Nano Lett* **2009,** *9* (12).

22. Nuzzo, R. G.; Allara, D. L. Adsorption of Bifunctional Organic Disulfides on Gold Surfaces. *J. Am. Chem. Soc.* **1983,** *105* (13), 4481-4483.

23. Nuzzo, R. G.; Dubois, L. H.; Allara, D. L. Fundamental-Studies of Microscopic Wetting on Organic-Surfaces .1. Formation and Structural Characterization of A Self-Consistent Series of Polyfunctional Organic Monolayers. *J. Am. Chem. Soc.* **1990,** *112* (2), 558-569.

24. Love, J. C.; Estroff, L. A.; Kriebel, J. K.; Nuzzo, R. G.; Whitesides, G. M. Self-assembled monolayers of thiolates on metals as a form of nanotechnology. *Chemical Reviews* **2005,** *105*, 1103-1169.

25. Schreiber, F. Structure and growth of self-assembling monolayers. *Prog. Surf. Sci.* **2000,** *65* (5-8), 151-256.

26. Banga, R.; Yarwood, J.; Morgan, A. M.; Evans, B.; Kells, J. Ftir and Afm Studies of the Kinetics and Self-Assembly of Alkyltrichlorosilanes and (Perfluoroalkyl)Trichlorosilanes Onto Glass and Silicon. *Langmuir* **1995,** *11* (11), 4393-4399.

27. Sugimura, H.; Hozumi, A.; Kameyama, T.; Takai, O. Organosilane self-assembled monolayers formed at the vapour/solid interface. *Surf. Interface Anal.* **2002,** *34* (1), 550-554.

28. Allara, D. L.; Parikh, A. N.; Rondelez, F. Evidence for A Unique Chain Organization in Long-Chain Silane Monolayers Deposited on 2 Widely Different Solid Substrates. *Langmuir* **1995,** *11* (7), 2357-2360.

29. Herrwerth, S.; Eck, W.; Reinhardt, S.; Grunze, M. Factors that determine the protein resistance of oligoether self-assembled monolayers - Internal hydrophilicity, terminal hydrophilicity, and lateral packing density. *J. Am. Chem. Soc.* **2003,** *125* (31), 9359-9366.

30. Yang, Z. H.; Galloway, J. A.; Yu, H. U. Protein interactions with poly(ethylene glycol) self-assembled monolayers on glass substrates: Diffusion and adsorption. *Langmuir* **1999,** *15* (24), 8405-8411.

31. Abbott, N. L.; Folkers, J. P.; Whitesides, G. M. Manipulation of the Wettability of Surfaces on the 0.1-Micrometer to 1-Micrometer Scale Through Micromachining and Molecular Self-Assembly. *Science* **1992,** *257* (5075), 1380-1382.

32. Ulman, A.; Evans, S. D.; Shnidman, Y.; Sharma, R.; Eilers, J. E.; Chang, J. C. Concentration-Driven Surface Transition in the Wetting of Mixed Alkanethiol Monolayers on Gold. *J. Am. Chem. Soc.* **1991,** *113* (5), 1499-1506.

33. Yamamoto, Y.; Nishihara, H.; Aramaki, K. Self-Assembled Layers of Alkanethiols on Copper for Protection Against Corrosion. *J. Electrochem. Soc.* **1993,** *140* (2), 436-443.

34. Sinapi, F.; Forget, L.; Delhalle, J.; Mekhalif, Z. Self-assembly of (3-mercaptopropyl)trimethoxysilane on polycrystalline zinc substrates towards corrosion protection. *Appl. Surf. Sci.* **2003,** *212*, 464-471.

35. Hintze, P. E.; Calle, L. M. Electrochemical properties and corrosion protection of organosilane self-assembled monolayers on aluminum 2024-T3. *Electrochim. Acta* **2006,** *51* (8-9), 1761-1766.

36. Sinapi, F.; Issakova, T.; Delhalle, J.; Mekhalif, Z. Study of (3-mercaptopropyl)trimethoxysilane reactivity on zinc: Comparison with organothiol and organosilane thin films. *Thin Solid Films* **2007,** *515* (17), 6833-6843.

37. Sinapi, F.; Lejeune, I.; Delhalle, J.; Mekhalif, Z. Comparative protective abilities of organothiols SAM coatings applied to copper dissolution in aqueous environments. *Electrochim. Acta* **2007,** *52* (16), 5182-5190.

38. Simon, R. A.; Ricco, A. J.; Wrighton, M. S. Synthesis and Characterization of A New Surface Derivatizing Reagent to Promote the Adhesion of Polypyrrole Films to Normal-Type Silicon Photo-Anodes - N-(3-(Trimethoxysilyl)Propyl)Pyrrole. *J. Am. Chem. Soc.* **1982,** *104* (7), 2031-2034.

39. Rubinstein, I.; Rishpon, J.; Sabatani, E.; Redondo, A.; Gottesfeld, S. Morphology Control in Electrochemically Grown Conducting Polymer-Films .1. Precoating the Metal-Substrate with An Organic Monolayer. *J. Am. Chem. Soc.* **1990,** *112* (16), 6135-6136.

40. Willicut, R. J.; Mccarley, R. L. Surface-Confined Monomers on Electrode Surfaces - Electrochemical and Microscopic Characterization of Omega-(N-Pyrrolyl)Alkanethiol Self-Assembled Monolayers on Au. *Langmuir* **1995,** *11* (1), 296-301.

41. Wu, C. G.; Chiang, S. C.; Wu, C. H. Formation and electrochemical property of pyrrole-terminated SAMs and the effect of the SAMs on the physicochemical properties of polypyrrole films electrochemically deposited over them. *Langmuir* **2002,** *18* (20), 7473-7481.

42. Dimitrakopoulos, C. D.; Malenfant, P. R. L. Organic thin film transistors for large area electronics. *Advanced Materials* **2002,** *14* (2), 99-+.

43. Horowitz, G. Organic thin film transistors: From theory to real devices. *J. Mater. Res.* **2004,** *19* (7), 1946-1962.

44. Yang, Y.; Ouyang, J.; Ma, L. P.; Tseng, R. J. H.; Chu, C. W. Electrical switching and bistability in organic/polymeric thin films and memory devices. *Advanced Functional Materials* **2006,** *16* (8), 1001-1014.

45. Angelopoulos, M. Conducting polymers in microelectronics. *Ibm Journal of Research and Development* **2001,** *45* (1), 57-75.

46. Forrest, S. R. The path to ubiquitous and low-cost organic electronic appliances on plastic. *Nature* **2004,** *428* (6986), 911-918.

47. Van Alsten, J. G. Self-assembled monolayers on engineering metals: Structure, derivatization, and utility. *Langmuir* **1999,** *15* (22), 7605-7614.

48. Supriya, L.; Claus, R. O. Solution-based assembly of conductive gold film on flexible polymer substrates. *Langmuir* **2004,** *20* (20), 8870-8876.

49. Widge, A. S.; Jeffries-El, M.; Cui, X. Y.; Lagenaur, C. F.; Matsuoka, Y. Self-assembled monolayers of polythiophene conductive polymers improve biocompatibility and electrical impedance of neural electrodes. *Biosensors & Bioelectronics* **2007,** *22* (8), 1723-1732.

50. Nalwa, H. S. *Handbook of Advanced Electronic and Photonic Materials and Devices;* Academic Press: **2001**.

51. Freund, M. S.; Lewis, N. S. A Chemically Diverse Conducting Polymer-Based Electronic Nose. *Proc. Natl. Acad. Sci. U. S. A.* **1995,** *92* (7), 2652-2656.

52. Q.Fang; D.G.Chetwynd; J.A.Covington; c.-S.Toh; J.W.Gardner . Micro-gas sensor with conducting polymers. Sensors and Actuators, B: Chemical Sensors and Materials. **2002,** 84, 66-71.

53. Cho, J. H.; Yu, J. B.; Kim, J. S.; Sohn, S. O.; Lee, D. D.; Huh, J. S. Sensing behaviors of polypyrrole sensor under humidity condition. *Sensors and Actuators B-Chemical* **2005,** *108* (1-2), 389-392.

CHAPTER 2

SELF-ASSEMBLED MONOLAYERS

2. SELF-ASSEMBLED MONOLAYERS

2.1 SELF-ASSEMBLY OF THIOLS ON GOLD SURFACES

2.1.1 INTRODUCTION

Self-assembled monolayers (SAMs) are the most elementary form of a nanometer-scale organic thin film material. Nuzzo and Allara are considered the pioneers of SAMs research since in 1983 they published the work *"Adsorption of Bifunctional Organic Disulfides on Gold Surfaces"*.[1] They reported a new technique to form well-ordered monolayers in contrast to the well-known Langmuir-Blodgett deposition. This new technique involved spontaneous organization of organic disulfides absorbed on freshly evaporated gold substrates. Since then, the preparation, formation, structure and applications of SAMs have gained much attention in the surface engineering field.

The most extensively studied system is derived from the adsorption of alkanethiols on gold surfaces. Thus, a considerably amount of literature is available on this issue. Especially interesting can be the book published by A. Ulman[2] or the most recent reviews published by Schreiber[3] or Love[4] for a general overview.

There are several reasons why the alkanethiol-gold system has been historically the most employed. Most of them stem from gold surface characteristics. Thin films of gold are quite simple to obtain either by physical vapour deposition, sputtering or electrodeposition. Gold is an inert metal. It does not oxidise at temperatures below its melting point and neither atmospheric oxygen nor most chemicals react with it. This enables to handle and manipulate samples under atmospheric conditions instead of ultra-high vacuum or clean room environment. Moreover, thin films of gold are compatible with a great number of existing spectroscopies and analytical techniques, such as, Surface Plasmon Resonance (SPR), QCM and Infrared Reflection Absorption Spectroscopy (IRRAS). In addition, gold has been proved to be compatible with living cells, in fact, cells can adhere and function on gold surfaces without evidences of toxicity.[5,6]

Besides, alkanethiols also favour the self-assembly process. Chemisorption of alkanethiols on gold yields monolayers by forming Au (I) thiolate (RS^-) species. The

reaction may be considered as an oxidative addition of the S-H bond to the gold surface, followed by a reductive elimination of hydrogen (Equation 1). The monolayer formation is enhanced by the thiol-gold bond strength, which was calculated to be ~40 kcal/mol.[7] Van der Waals interactions among adjacent chains also contribute to stabilise the monolayer by 1.5 kcal/mol per methylene.

$$R-SH+Au_n^0 \rightarrow R-S^- - Au^+ \cdot Au_{n-1}^0 + \tfrac{1}{2} H_2 \qquad (1)$$

Related to the monolayer structure, thiol head groups are attached to the threefold hollow site forming a $\left(\sqrt{3}\times\sqrt{3}\right)R30^o$ configuration on the hexagonal close-packed Au {111} surface. However, a combined He atom and X-ray diffraction study revealed a c(4x2) superlattice, by which in an unit cell, two molecules display slightly different orientations when compared with the other two.[8] It has a sulphur spacing of 4.97 Å, resulting in an available area for each molecule of 21.4 Å^2. Since the Van der Waals diameter of the alkane chain is somewhat small (4.6 Å) for the chain to completely occupy that area, the chains will tilt forming an angle of approximately 30° with the surface normal. Moreover, chains are disposed predominantly in *trans* conformation to achieve an optimal packing and maximize Van der Waals interactions.

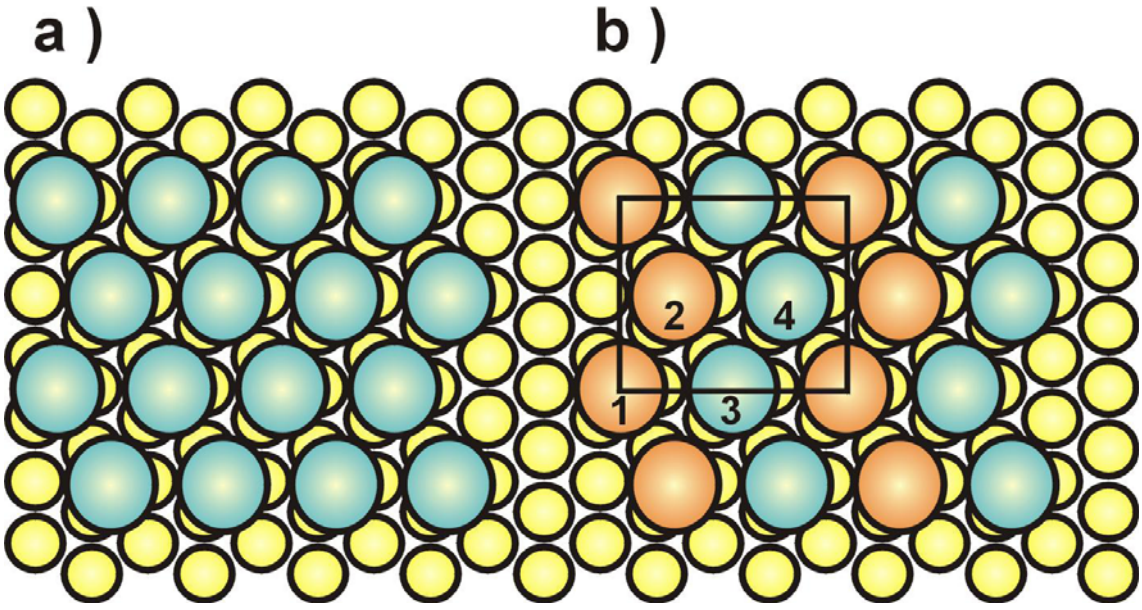

Figure 1. The small circles represent the gold atoms and the big ones the alkanethiol molecules. A) Scheme of the (√3 x √3) structure of alkanethiols on gold. B) Scheme of the c(4 x 2) superlattice in which 1 and 2 molecules are equivalent but different to 3 and 4 (Barrena, 2001).

In this first part, we decided to work with this archetype thiol-gold system. The behaviour of this monolayer has been widely described and the thiolate bond has been shown to form high quality monolayers, as commented above. Because of this, this system was chosen to perform the first experiments on surface modification and polymerization.

2.1.2 EXPERIMENTAL PART

2.1.2.1 Chemicals

1,3-Dibromopropane (99%) was purchased from Fluka; 1,6-dibromohexane (96%), 1,12-dibromododecane and thiourea (99%) were obtained from Aldrich and were used without further purification. Pyrrole (98%) was purchased from Aldrich and was purified by distillation. KOH (85%), absolute ethanol, HCl (37%), H_2SO_4 (96%), H_2O_2 (30%) and CH_2Cl_2 (99.5%) were purchased from Panreac; THF (99.9%) and diethyl ether (99.7%) from Aldrich; ethyl acetate (99%) and petroleum ether from Carlo Erba and $MgSO_4$ from Quimivita, all of them were used as received.

2.1.2.2 Synthesis of ω-(N-pyrrolyl)alkanethiol

Different homologues of ω-(N-pyrrolyl)alkanethiol (n = 3, 6, 12) have been synthesized to be used as SAM's promoters (Scheme 1). Their synthesis based on previous investigations[9-11] is described next.

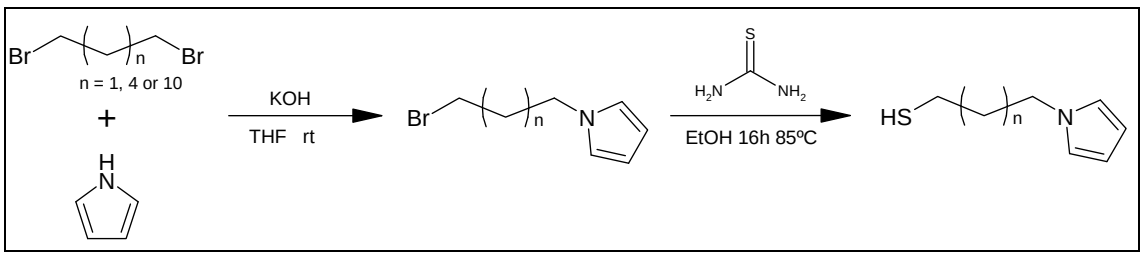

Scheme 1.

In a 100 ml round-bottom flask, 20 mmol dibromoalkane, 20 mmol of KOH powder and 50 mmol of dibromoalkane were added in 50 ml of dry tetrahydrofurane (THF). The reaction mixture was stirred overnight in a nitrogen atmospher. Deionized water (50 ml) was added and the product was extracted with diethyl ether (4x25 ml). The organic

phase was dried with anhydrous $MgSO_4$, filtered and evaporated under reduced pressure to obtain N-bromoalkylpyrrole.

Afterwards, in a 50 ml round-bottom flask, 2 mmol of N-bromoalkylpyrrole and 11 mmol of thiourea were added to 50 ml of ethanol. This mixture was heated under reflux at 85 ºC for 16 h. Ethanol was removed by distillation under reduced pressure. Next, 50 ml of 0.3 M KOH aqueous solution was added, and the mixture was heated under reflux at 90 ºC for 3 h. Finally, the reaction mixture was quenched with a 100 ml 0.1 M HCl solution. The product was extracted with CH_2Cl_2 (4x25 ml). Solvent was removed by distillation under reduced pressure. The product was purified by flash chromatography on silica gel (240-400 mesh) using petroleum ether/ethyl acetate (50:1) as eluent to give ω-(N-pyrrolyl)alkanethiol, as a transparent liquid.

3-(N-pyrrolyl)propanethiol (Py3SH), 38% yield.

^{1}H-NMR ($CDCl_3$, 200 MHz): δ 1.34 (t, 1H, SH), 2.07 (m, 2H, C2), 2.47 (m, 2H, C1), 4.03 (t, 2H, C3), 6.15 (t, 2H, ArH), 6.65 (t, 2H, ArH).

FT-IR ($CHCl_3$, υ/cm^{-1}): 3092 (arom C-H), 2927 (υ_{as} CH_2), 2856 (υ_s CH_2), 2550 (SH), 1546-1460 (pyrrole ring), 1359 (C-N).

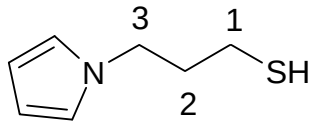

6-(N-pyrrolyl)hexanethiol (Py6SH), 37% yield.

^{1}H-NMR ($CDCl_3$, 200 MHz): δ 1.31 (m, 5H, C3-4, SH), 1.58 (m, 2H, C2), 1.74 (m, 2H, C5), 2.50 (m, 2H, C1), 3.85 (t, 2H, C6), 6.12 (t, 2H, ArH), 6.64 (t, 2H, ArH);).

FT-IR ($CHCl_3$, υ/cm^{-1}): 3098 (arom C-H), 2930 (υ_{as} CH_2), 2856 (υ_s CH_2), 2552 (SH), 1540-1460 (pyrrole ring), 1370 (C-N).

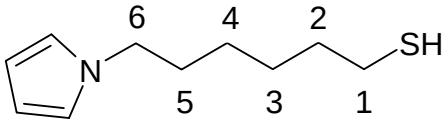

12-(N-pyrrolyl)dodecanethiol (Py12SH), 41% yield.

^{1}H-NMR ($CDCl_3$, 200 MHz): δ 1.27 (m, 17H, C3-10, SH), 1.62 (m, 2H, C2), 1.76 (m, 2H, C11), 2.55 (q, 2H, C1), 3.86 (t, 2H, C12), 6.13 (t, 2H, ArH), 6.64 (t, 2H, ArH).

FT-IR ($CHCl_3$, υ/cm^{-1}): 3100 (arom C-H), 2925 (υ_{as} CH_2), 2853 (υ_s CH_2), 2553 (SH), 1540-1464 (pyrrole ring), 1370 (C-N).

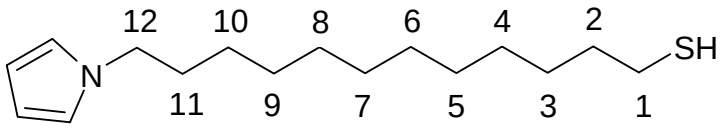

2.1.2.3 Substrate preparation

The surfaces in which the self assembly was carried out consist of a silicon wafer substrate, a thin chromium layer and a gold layer. The chromium layer is used to promote adhesion of the gold film to the underlying substrate. Chromium (2.5 nm) and gold (85.50 nm) were thermally evaporated onto the silicon wafer substrates (surface RMS roughness 6.4 nm). The deposition was carried out at a pressure less than $3x10^{-7}$ Torr. Freshly gold substrates were cleaned in a piranha solution (70% H_2SO_4 and 30% H_2O_2 (30% H_2O_2 in H_2O)) for 30 min. Finally the substrate was rinsed thoroughly with deionised water and absolute ethanol immediately prior monolayer formation.

2.1.2.4 The self-assembly

Assembly of the monolayer was obtained by dipping the gold substrate into a 1 mM solution of ω-(N-pyrrolyl)alkanethiol. After 24 hours the substrate was removed, sonicated for 10 minutes in ethanol and rinsed extensively with ethanol absolute, in order to remove the possible physisorption of the monomer on the top of the monolayer. Finally, the gold substrate was blown dry with nitrogen. Samples were stored under argon atmosphere until further characterization or polymerization.

2.1.2.5 Equipment and methods

NMR spectra were recorded on a Varian Gemini 300 HC apparatus.
FT-IR spectra were collected on a Nicolet Magna 560 FTIR spectrophotometer.
XPS was carried out in a PHI 5500 Multitechnique System (Physical Electronics) with a monochromatic X-ray source (Aluminium Kalfa line of 1486.6 eV energy and 350 W), placed perpendicular to the analyzer axis and calibrated using the 3 $d_{5/2}$ line of Ag. The analyzed area was a circle of 0.8 mm diameter. The XPS spectra were analyzed by the Multipack Version 5.0A software. All spectra were referenced to the Au (4 $f_{7/2}$) peak at 84 eV. The peaks were analysed using mixed Gaussian-Lorentzian curves (80% of

Gaussian character). The sulphur doublets were fitted using an intensity ratio and energy separation of 2:1 and 1.18 eV, respectively.

The electrochemical measurements were made in a Gamry PC3-300 potentiometer and graphs were analyzed by the CMS 100 software. The experiments were performed in a three-electrode cell, using the gold surface or the SAM-modified gold as the working electrode, a saturated KCl Ag/AgCl reference electrode and a platinum electrode as the counter electrode. The voltammograms were measured in a 0.1 M KCl solution, with a scan range from -1 to +1.8 V and at a scan rate of 100 mV/s. For the polymerization curves the solution used was 0.1 M KCl containing 0.02 M pyrrole monomer.

The TOF-SIMS analysis was performed using a TOF-SIMS IV mass spectrometer (ION-TOF, Munster, Germany) operated at a pressure of 5 x 10-9 mbar, 18 ns pulses of 25 keV Bi3+ (primary ions) were bunched, with an incidence angle of 45º, to form ion packets with a nominal temporal extent of <0.9 ns at a repetition rate of 10 kHz, which produced a target current of 0.2 pA. These primary ion conditions were used to scan a 125x125 μm area of the sample for 30 s.

2.1.3 SAM CHARACTERIZATION

Monolayer formation was studied using different techniques. X-Ray Photoelectron Spectroscopy (XPS) was used to determine the binding energy between the thiol group and the gold substrate and the quantitative atomic composition on the surface. The Cyclic Voltammetry (CV) was performed to evaluate the quality of monolayer protection. Time of Flight Secondary Ion Mass Spectrometry (TOF-SIMS) provided a more detailed characterization of the chemical composition on the surface.

2.1.3.1 XPS

The XPS analysis was performed in the three monolayers formed to study their chemical state. It should be noted that PY6SH SAM was left 10 weeks in air before the analysis in order to evaluate its stability.

The survey XPS spectra of Py3SH, Py6SH and Py12SH SAMs on gold (Figure 2, Figure 3 and Figure 4) show typical features for these samples. The characteristic peak for gold (Au 4f) is observed at 84 eV, the sulphur atom (S 2p) is found at 163 eV, the

carbon (C 1s) signal at 285 eV, the nitrogen (N 1s) at 400 eV and the oxygen (O 1s) at 431 eV.

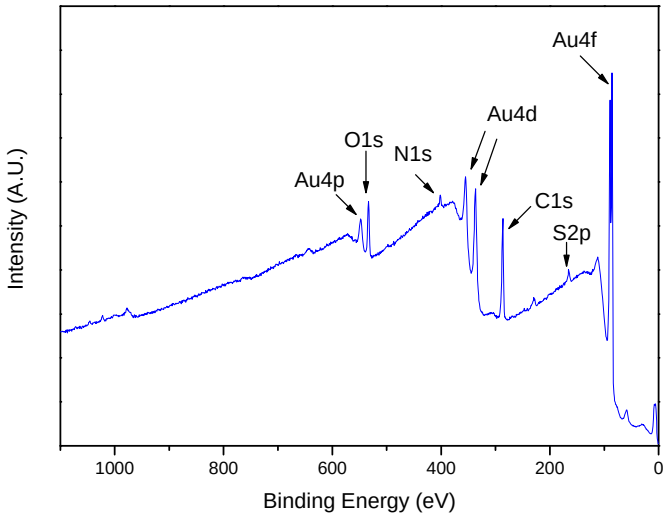

Figure 2. XPS spectrum of Py3SH monolayer on gold

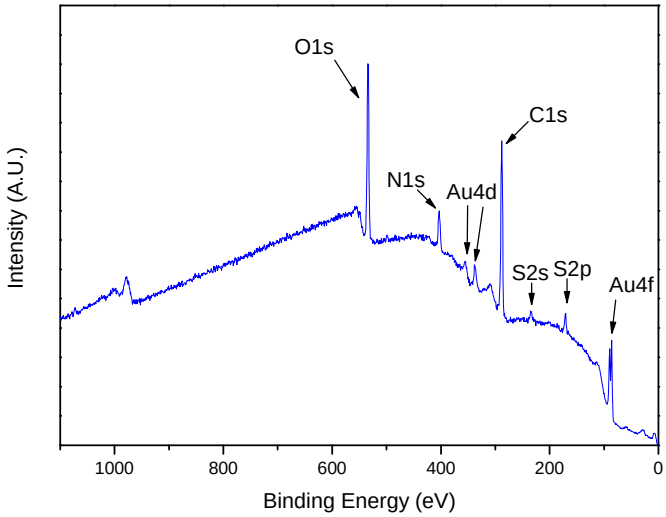

Figure 3. XPS spectrum of Py6SH monolayer on gold

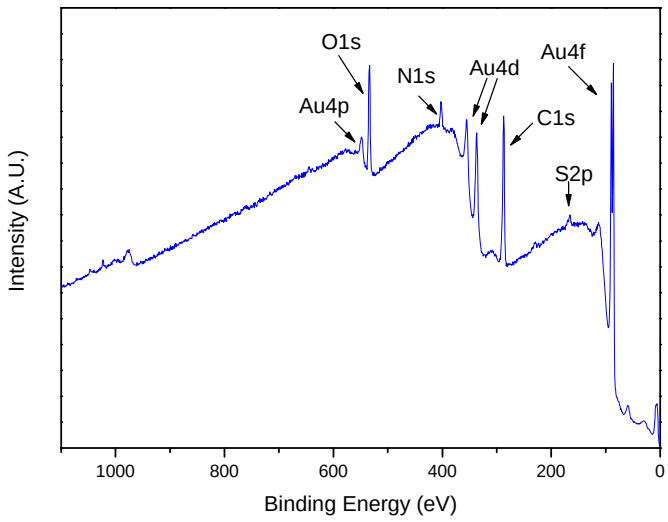

Figure 4. XPS spectrum of Py6SH monolayer on gold

The surface composition of the three ω-(N-pyrrolyl)alkanethiol monolayers is presented in Table 1. The most striking result is the high concentration of oxygen found on the surface, especially in Py6SH SAMs. This can be due to atmospheric contaminants or oxidized species. Because of that, it makes the correlation study among atoms more difficult. Table 2 shows the C/N, C/S, O/C and N/S ratios of the different surfaces. The experimental C/S ratios are 16.7, 20.0 and 18.0 for Py3SH, Py6SH and Py12SH SAMs, however the theoretical value should be 7, 10 and 16 respectively. In all samples, the measured value is higher than expected estimations, especially for Py3SH and Py6SH. These results suggest that there is an additional source of carbon apart from the monolayer samples which is thought to be contaminants. Additionally, the N/S theoretical ratio for all the monolayers is 1, whereas the experimental ratio is slightly higher for all of them. In general, composition and ratio of the Py12SH monolayer are quite close to the expected values, which confirms the self-assembly. By contrast, there are some differences for Py3SH and Py12SH SAMs, which could be explained by surface oxidation or contamination. Therefore, in order to determine the causes of these differences the deconvolution analysis is presented next.

Table 1. XPS surface composition of the different substrates.

	Py3SH	Py6SH	Py12SH
C (1s)	63.4	60.6	62.9
N (1s)	4.5	9.3	7.3
O (1s)	12.7	25.2	16.8
S (2p)	3.8	3.0	3.5
Au (4f)	15.6	1.9	9.5

Table 2. XPS ratios of C/N, C/S, O/C and N/S.

	Py3SH	Py6SH	Py12SH
C/N	14.2	6.5	8.6
C/S	16.7	20.0	18.0
O/C	0.2	0.4	0.3
N/S	1.2	3.1	2.1

XPS deconvolution analysis

The chemical bond between gold and thiol has been intensely studied by XPS and many studies have been published during the last years about this issue.[12-18] Thiolate bond formation has been reported to be observed at 162 eV. The XPS spectrum in this region shows the presence of $S2p_{3/2}$ and $S2p_{1/2}$ peaks at 162 and 163.2 eV respectively, due to the spin-orbital splitting effect. The spectrum is fitted using a 2:1 peak area ratio with a splitting of 1.18 eV. Moreover, an additional peak is observed at 163.7 eV. This binding energy can be assigned to unbound thiols or to the resulting disulfide,[19,20] and it has been fit as a doublet as well. In addition, another peak at 168 eV has been observed in all the samples. This signal is assigned to sulfonate species. The appearance of this chemical group can be explained due to oxidation of organothiol SAMs in contact to air to yield sulfonates.[21-23] After long exposure to air, the thiol signal decreases, while the sulfonate one increases. In order to study the different chemical states of the sulphur, a deconvolution analysis on the S 2p peak has been performed. The high resolution S 2p spectra of Py3SH, Py6SH and Py12SH monolayers are shown in Figure 5, Figure 6 and Figure 7.

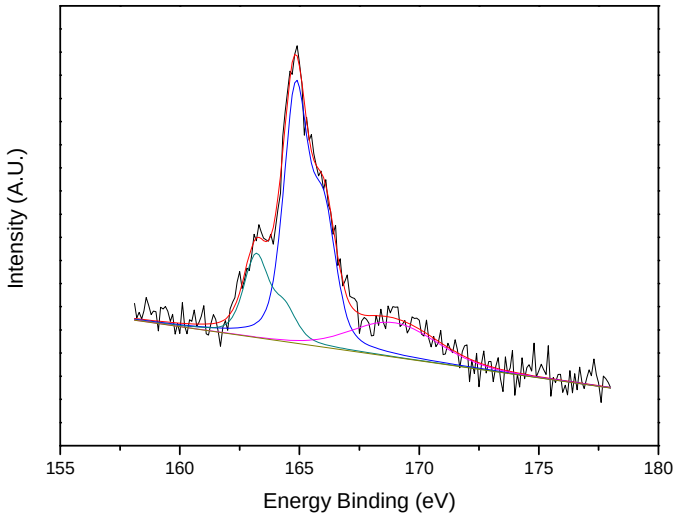

Figure 5. S 2p high resolution XPS spectrum of Py3SH

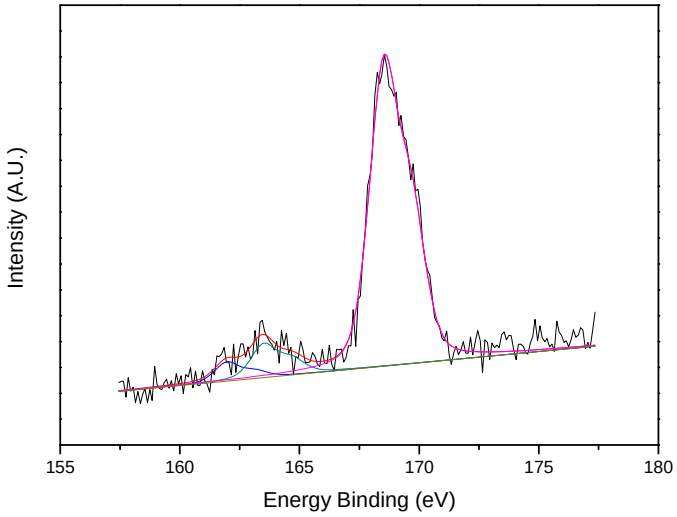

Figure 6. S 2p high resolution XPS spectrum of Py6SH

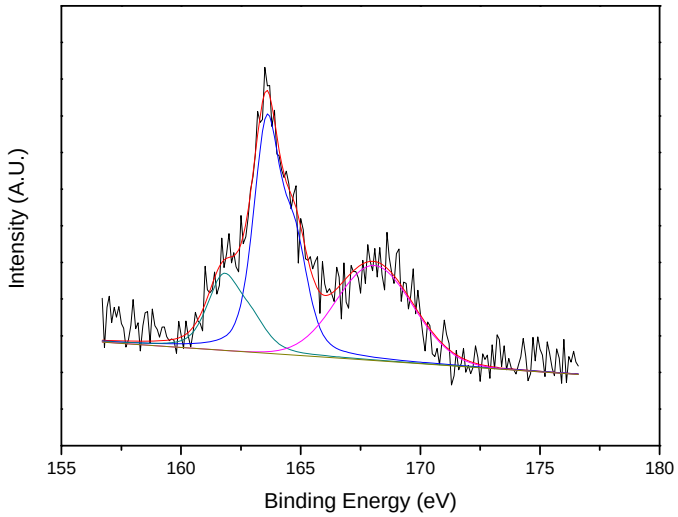

Figure 7. S 2p high resolution XPS spectrum of Py12SH

The deconvolution analysis shows that only a low percentage of thiol molecules are bound to the gold substrate (Table 3). In Py3SH and Py12SH SAMs, the highest intensity peak belongs to the unbound thiol or disulfide. The thiol and the disulfide chemical group present a very close binding energy, which make them undistinguishable even by high resolution XPS. The disulfide molecule can be found in thiol solutions due to oxidation of the –SH group by exposure to atmospheric oxygen. Furthermore, results suggest a considerable amount of sulfonate species in both samples. The presence of the sulfonate groups can explain the lower thiolate percentage. As long as thiol molecules are oxidized to yield the sulfonate, the thiolate peak decreases its intensity. Additionally, Castner[20] demonstrated that an unrinsed or insufficient rinsed of the sample and a high-concentred thiol solution can lead to an excess of unbound thiol. Despite having rinsed the sample several times with absolute ethanol, it seems that not all the unbound thiols or disulfides have been removed. The possible $\pi \rightarrow \pi$ interactions among the electronic clouds of the pyrrole rings can decrease the efficiency of the washing step, making the rinse more difficult and resulting in a higher percentage of unbound thiol in our samples. Therefore, the unbound thiol percentage is higher than expected. Another reason could be the contamination of the gold surface which would make the assembly between thiol and gold more difficult.

Table 3. Binding energies and quantitative analysis (%) of the S 2p and C 1s chemical bond corresponding to Py3SH, Py6SH and Py12SH monolayers.

		Py3SH		Py6SH		Py12SH	
		B.E. (eV)	%	B.E. (eV)	%	B.E. (eV)	%
S 2p	S-Au	162.0	18.1	162.0	4.1	161.8	15.8
	S unbound / S-S	163.7	63.5	163.5	8.9	163.6	47.8
	S ox	168	18.4	168.5	87	167.7	36.4
C 1s	C-C	284.9	70.1	285	43.4	285	57.8
	C-N	285.7	7.7	286	14.7	285.9	13.4
	C-O-C	286.5	12.0	286.7	35.6	286.4	13.5
	C oxid	288.1	10.2	288.2	6.3	288	15.3

As stated before, the *a priori* unexpected sulfonate peak can be explained by an excessive exposure to air before the XPS analysis. Several days in contact to air can cause the appearance of this peak. To corroborate this hypothesis, the Py6SH sample was left in contact with air 10 weeks before performing the XPS analysis. As shown in Table 5, most of the S 2p signal corresponds to the sulfonate specie (87%), while the thiolate, unbound thiol or disulfide are found in a very low concentration. These results confirm the evolution from thiol to sulfonate by a progressive oxidation of the monolayer anchoring group.

In addition, the C 1s high resolution spectra of the different monolayers have been included to complete the chemical information (Figure 8, Figure 9 and Figure 10). The carbon signal has been split into four peaks. The peak at 285 eV (C-C) originates from the carbons that form the monolayer (except the ones bounded to the nitrogen atom) and the peak at 286.0 eV (C-N) corresponds to the carbon atoms linked to the nitrogen of the pyrrolyl group. Then, two different peaks were assigned to different oxidized carbon species. The feature at 286.6 eV (C-O-C) is attributed to alkoxy groups and the peak at 288.0 eV (C_{ox}) to other oxidized species such as -COO-. The results for the monolayer analysis can be seen in Table 3.

The theoretical ratios between the C-C and the C-N peaks are 1.33, 2.33 and 4.33 for the Py3SH, Py6SH and Py12SH SAMs respectively and the observed ratios are 9.10, 2.95 and 4.31. As it can be seen, the C-C/C-N ratio which best fits is observed for the Py12SH SAM, whereas the Py6SH ratio is slightly higher and the Py3SH considerably higher. This observation agrees with the XPS composition analysis described previously. The reason for this high discrepancy can be explained by a poor

organization of the monolayer. If the monolayer is not compact enough, the adsorption of atmospheric contaminants can take place. Thereby, the aliphatic carbons of the atmospheric contaminants increase the C-C peak which theoretically is attributed to carbons from the monolayer only.

Furthermore, it is interesting to remark the alkoxy peak at 286.6 eV. While Py3SH and Py12SH SAMs present similar intensity values (12% and 13.5%), the Py6SH SAM shows a significantly higher value (35.6%). It should be taken in account that the Py6SH sample was left exposed to air for a long period of time to observe its effect on the monolayer. As it was discussed before, it entails the appearance of sulfonate groups. Nevertheless, this result suggests the formation of alkoxy species, besides other oxidized species, due to the monolayer oxidation. Thus, the presence of the alkoxy peak in the monolayers indicates an oxidation process which can affect the monolayer quality and it could explain the low thiol-gold binding.

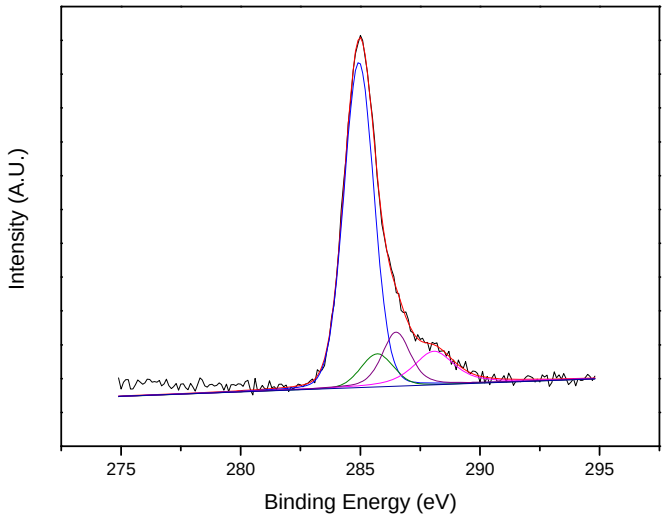

Figure 8. C 1s high resolution spectrum of Py3SH.

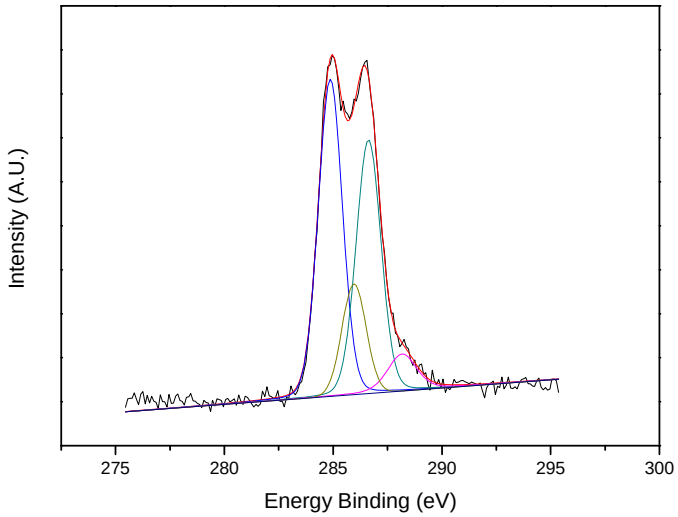

Figure 9. C 1s high resolution spectrum of Py6SH.

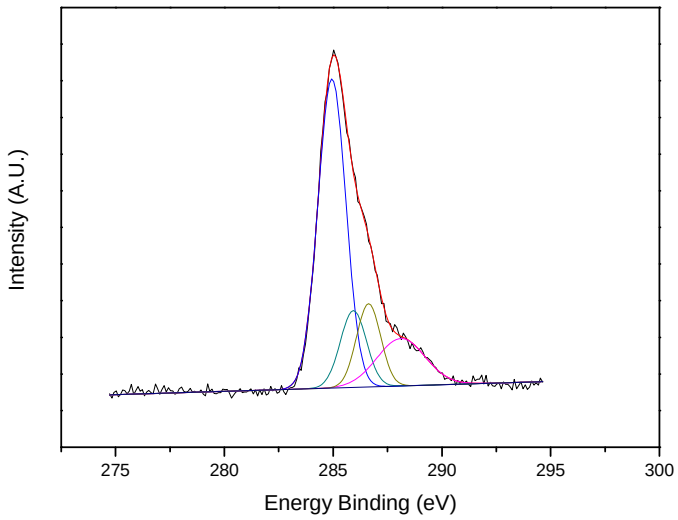

Figure 10. C 1s high resolution spectrum of Py12SH.

2.1.3.2 Cyclic voltammetry

CV is a powerful tool to study the electrochemistry on a surface. Therefore, it has been extensively used to investigate the monolayer structure. This technique can determine the charge transfer process at the interface which is influenced by the nature of the

electrode surface. Comparing the voltammogram between unmodified substrate and SAM-modified gold, it is possible to study the effect of the SAM in aqueous solutions.

After carrying out the CV on unmodified gold, it was observed that the gold film had been removed from the silica substrate in our experiments. The formation of oxygen gas in the anodic scan due to the oxidation of water (Equation 2) lead to a cavitation attack causing the detachment of the gold film.

$$H_2O \rightarrow 2H^+ + \frac{1}{2}O_2 + 2e^- \quad \text{E = 1.23 V} \tag{2}$$

Formation of oxygen bubbles produced a physical attack at the edge of the substrate; thus it can be assumed that friction can be the cause of the peeling off. As a consequence, no data for these experiments could be recorded. In contrast, no detachment was observed for SAM-modified gold electrodes when the CV was performed. A typical voltammogram for a SAM-modified electrode is presented in Figure 11. An irreversible oxidative peak is observed at around 1.2 V. Chloride solutions under anodic potential cause gold dissolution due to an oxidative reaction (Equation 3). In addition, the monolayer desorption process seems to appear near of this potential. The cleavage of the thiolate bond can be achieved by applying a specific voltage on the monolayer.

$$Au + 4Cl^- \rightarrow AuCl_4^- + 3e^- \quad \text{E = 1.2 V} \tag{3}$$

Since these two processes present a similar potential, it is not possible to distinguish them in the voltammogram. Furthermore, at this point, it would not be possible to assure which one of the two processes occurs first. It is possible that gold dissolution lead to the monolayer desorption. Or, that due to the monolayer desorption, the gold surface is exposed to the chloride solution and then, it helps the oxidation and posterior gold dissolution.

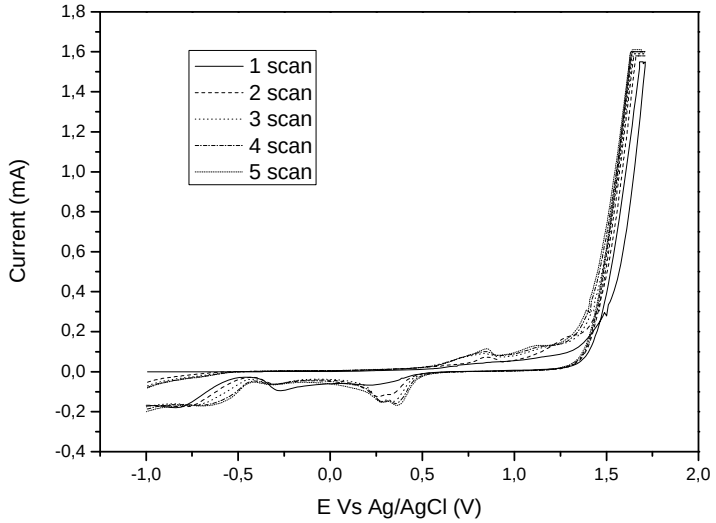

Figure 11. Cyclic voltammetry of Py6SH SAM on gold in a 0.1 M KCl solution. Scan range: from -1.0 to 1.8 V, scan rate: 100mV/s

Another irreversible oxidation peak at 0.8 V appears in the voltammogram, which can be assigned to the electropolymerization of the monolayer. The first attempt of an electrochemical polymerization of a monomer monolayer formed by self-assembly of a ω-(N-pyrrolyl)alkanethiol on Au was reported by Willicut and McCarley.[24] Cyclic voltammetries were performed in nonaqueous electrolyte solution obtaining an irreversible peak at E = +1.0 V Vs SSCE, corresponding to the oxidation of N-alkylpyrroles. Nevertheless, further experiments performed on aqueous electrolyte solution confirm the oxidation potential obtained in our experiments.[11,25] Once pyrrole groups are activated by electrochemical oxidation, side pyrrole units can be linked through 2 and 5 positions to form a PPy layer.

After CV of the monolayer was performed, deposition of PPy by CV on Py12SH SAM-modified gold surfaces was attempted. Although PPy deposition on SAM surfaces has been demonstrated, Collard *et al* reported that long alkylthiol monolayers on gold can difficult the polymerization process due to a reduction of the transport of redox active species in solution caused by surface electrode blockage.[26] Figure 12 shows the voltammogram for the PPy electropolymerization. The curves resemble the graph obtained during SAM characterization, except for the peak that appears at 1.1 V. The only difference in the experimental part was the introduction of pyrrole in the solution. Therefore, this peak can only be assigned to the pyrrole oxidation. Besides, it can be observed that after the first scan, there is no evidence of the peak. The explanation is

related to the mechanism of electrochemical polymerization. The first step to obtain a PPy film is to produce pyrrole active species to initiate the polymerization. These precursors are formed during the first scan. Then, during the second scan, activated pyrrole species react to yield short PPy chains. Finally, subsequent scans produce new reactive species that combine themselves to extend the polymer chain. For this reason, it is not possible to observe the PPy oxidation peak until the second scan. The oxidation peak intensity increases gradually, indicating that a higher amount of PPy is produced after each scan.

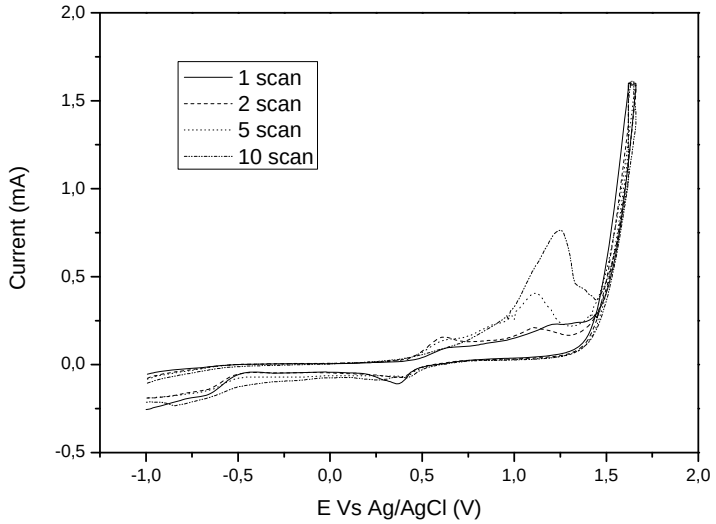

Figure 12. Cyclic voltammogram of electrodeposition of polypyrrole on Py12SH SAM-modified gold in 0.1 M KCl aqueous solution at a scan rate of 100 mV/s.

In a typical PPy polymerization performed by CV (Figure 13) a series of reduction peaks, which have not been found in our experiments, can be observed. In the oxidative scan, there are two peaks. The first one corresponds to the pyrrole oxidation and the second one to the chain oxidation. In the reductive scan, and approximately at the same potential than the polymer oxidation, there is a reduction peak, which corresponds to the reduction of the polymeric chain. The complete cycle includes the monomer oxidation, the chain oxidation and the chain reduction, without one of these steps it is not possible to achieve the electrochemical synthesis of PPy.

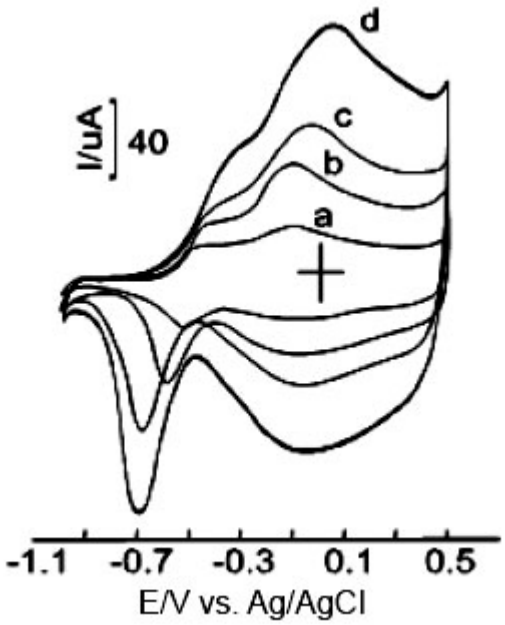

Figure 13. Cyclic voltammograms for polypyrrole polymerization (Arrieta, 2009)

Since the reduction step has not been observed in the electrochemical polymerization performed on the SAM-modified gold, it can be deduced that PPy mechanism formation has not been completed. It can be hypothesised that the oxidative peak observed at 1.1 V in Figure 12 belongs only to the pyrrole oxidation. The reason for this may stem from the protective effect of the monolayer, which blocks the electron transference and, as a consequence, it prevents the oxidation and reduction of the polymer chain. However, the pyrrole molecule has been demonstrated to be oxidised in the experiment. This oxidation can be due to a diffusional controlled reaction, where the monomer can get approach to the electrode. Pyrrole solubilised in water can diffuse through the monolayer to reach the surface electrode, where the electronic transference is more feasible. Then, the species are activated and, when they are close enough, they can react with each other to form polypyrrole. After that, more pyrrole species can reach the electrode surface, displacing the previously oxidised, and they can be oxidised to start the process again.

CV has demonstrated the insulator effect of the monolayer in the polymerization process. Although the high percentage of unbound thiol discussed in the XPS results, the electrochemical experiments prove that the thiolate-gold bond has been achieved as well and that the monolayer quality is still good enough. Moreover, it suggests that electrochemical polymerization is not the most viable way to deposit PPy on the monolayer. Thus, these results support the initial idea of performing plasma polymerization to deposit PPy thin films on SAM-modified substrates.

2.1.3.3 TOF-SIMS

SAMs were analyzed by TOF-SIMS in order to characterize their structures. Despite the fact that XPS or vibrational spectroscopies have been widely used to determine their bonding or their structure, TOF-SIMS can provide valuable information as well. While other techniques have limited spatial resolution, TOF-SIMS can supply a high mass range and a high sensitive analysis. For this study, this mass spectrometry technique has been used to confirm the monolayer formation. When the surface is bombarded by energetic primary particles (Bi^{3+}), secondary particles of different nature such as electrons, neutrals species atoms or molecules and atomic and cluster ions are emitted. The secondary ions are the ones which are detected and analyzed by a mass spectrometer. Thus, this process enables a detailed chemical analysis of the surface.

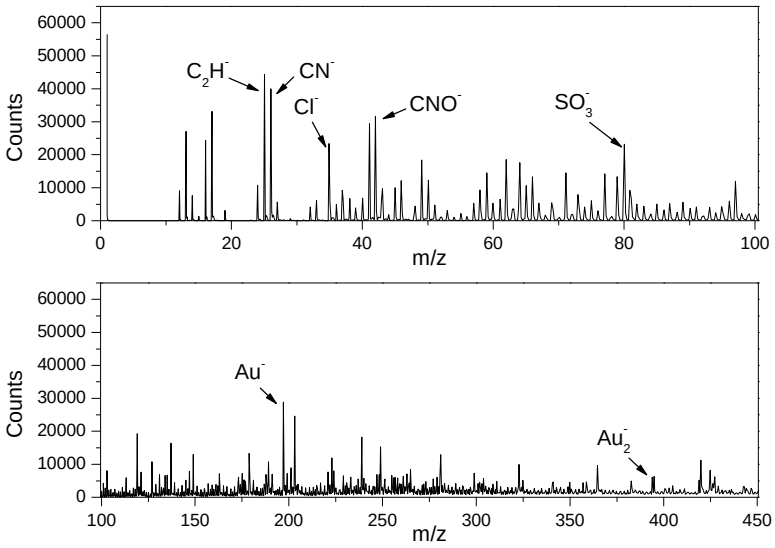

Figure 14. TOF-SIMS spectra of the gold surface. Upper spectrum ranges from m/z 0 to 100 and lower spectrum from 100 to 450.

The analysis was done by comparing characteristic features on bare gold and on SAM-modified gold surfaces (Figure 14, Figure 15 and Figure 16). Tarlov and Newman[27] were the first ones who studied SAMs by SIMS, focusing on methyl terminated monolayers of several chain lengths and describing many of the important spectral features. They reported the appearance of elemental ions Au^- (m/z = 197) and S^- (m/z = 32), together with SH^- (m/z = 33) as characteristic features to be taken into account. A range of gold-sulphur fragments were also observed: Au_2^-, AuS^-, AuS_2^-, Au_2S^- and

$Au_2S_2^-$ at an m/z of 394, 229, 261, 426 and 458 respectively. In addition, they reported a number of peaks that could be specifically associated with ions containing entire adsorbate molecules, which are: $(M\text{-}H)^-$, AuM^-, $AuMS^-$, $Au_2(M\text{-}H)^-$ and $Au(M\text{-}H)_2^-$ (being M the molecule adsorbed onto the surface). However, there was no evidence of such fragments in the surveyed spectra. Since the molecules that form the monolayer are ω-functionalised alkylthiols, it could be assumed that after the ion impact, fragmentation of this kind of SAMs do not follow the model proposed by Tarlov and Newman. Probably, the pyrrole group was removed from the alkyl chain and the peaks do not correlate with the predicted ones. Chemical differences in the composition of the monolayers lead to different fragmentation profiles. Thereby some of the ions studied by Tarlov and Newman can not be compared with the ones obtained in the pyrrole-terminated monolayers.

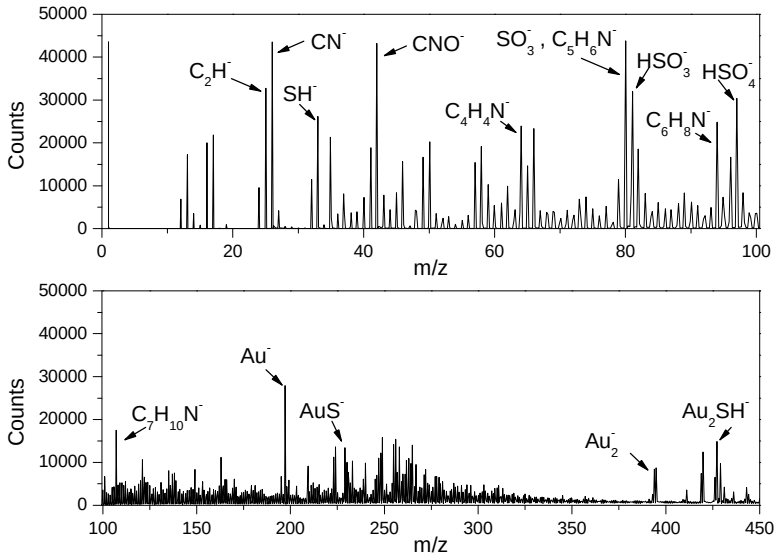

Figure 15. TOF-SIMS spectra of the Py3SH SAM on gold. Upper spectrum ranges from m/z 0 to 100 and lower spectrum from 100 to 450.

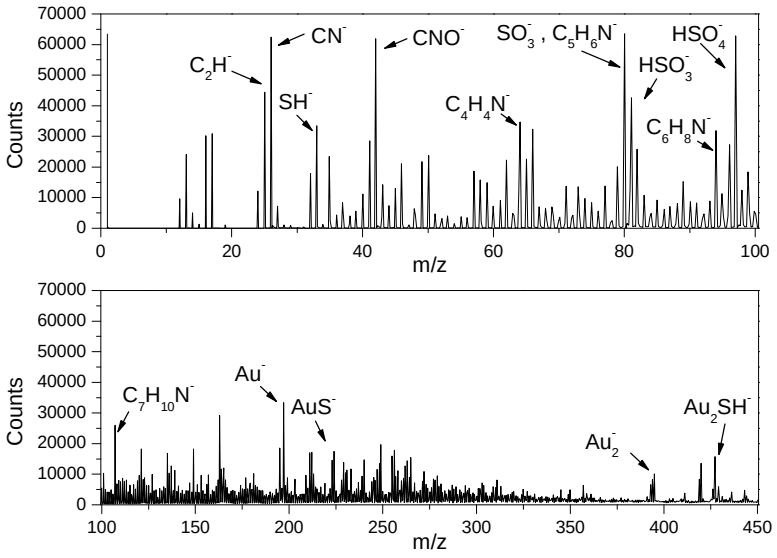

Figure 16. TOF-SIMS spectra of the Py12SH SAM on gold. Upper spectrum ranges from m/z 0 to 100 and lower spectrum from 100 to 450.

As a consequence, other fragments have been considered for the analysis. Table 4 shows the characteristics features of the monolayers in comparison with the same peaks in the bare gold. Obviously, the thiol group has been considered as one of the characteristic peaks. Another selected feature is the pyrrole group, which appears clearly on spectra of SAM-modified surfaces. As it was explained before, the pyrrole moiety could have been removed from the monomer and this fragment could be a good indicator of the monolayer assembly (m/z = 66). In the same way, the pyrrole group plus some methylenes could have been fragmented by the ion impact and, therefore, the N-alkylpyrrole family was analysed. These features have been studied in the three samples: unmodified gold surface, Py3SH and Py12SH SAMs. All the intensities were normalised to the Au^- ion (m/z = 197).

Table 4. Intensity ratio of the characteristic features against Au^-.

		Intensity		
Fragment	**m/z**	**Au**	**Py3SH**	**Py12SH**
SH^-	33	0.21	0.95	1.00
$C_4H_4N^-$	66	0.46	0.85	0.97
$C_5H_6N^-$	80	0.80	1.59	1.92
$C_6H_8N^-$	94	0.10	0.90	0.97
$C_7H_{10}N^-$	108	0.06	0.24	0.28

The thiol intensity ratio of the SAM-modified surfaces was approximately five times higher than the unmodified gold surface, which proves the assembly of the molecules on the surface. The pyrrole (m/z = 66) and the methylpyrrole (m/z = 80) fragment presented a high intensity, but it should be noticed that the intensity of the same signal on gold was quite high as well. For this reason, a careful interpretation of these signals should be done. Special attention should be given to the $C_5H_6N^-$ fragment, because at the same m/z there is another peak that can interfere with the results. The exposure of SAMs to air for extended periods can cause the oxidation of the immobilized structures. As it was reported in the XPS analysis, the thiol group can be oxidised to yield sulfonates. The appearance of peaks at m/z 80 and 97 (SO_3^- and HSO_4^-) is indicative of oxidation of the SAMs. Thus, the signal at m/z 80 is the sum of intensities of $C_5H_6N^-$ and SO_3^- fragments. This is the reason why the signal intensity for this fragment is so high. Nevertheless, SAM-modified samples show higher intensities than non-modified gold surfaces. Furthermore, the same occurs for the ethylpyrrole fragment (m/z = 94), which shows a low intensity in the gold surface and a higher one in the SAM-modified gold. On the whole, these results corroborate the idea that a number of homologues of N-alkylpyrroles are formed due to SAM fragmentation. The next fragments ($C_7H_{10}N^-$) show a lower intensity in compared with the previous one. It could be owed to the number of methylenes linked to the pyrrole; it is more likely to detect fragments with a shorter alkyl chain, because multiple collisions tend to fragment the longest molecules.

In general, higher intensities are observed in Py12SH SAMs compared to Py3SH. This phenomenon can be explained by the presence of a higher amount of 12-(N-pyrrolyl)dodecanethiol molecules on the monolayer. As a consequence, a higher density of material deposited on the monolayer induces more fragmentation and therefore, higher intensities.

2.1.3.4 Final remarks

On the whole, the thiol-gold system results in high quality monolayers. Nevertheless, the results obtained in this section have shown a SAM quality worse than expected, especially Py3SH and Py6SH SAMs. A lower purity of target molecules, a longer exposure to air before analysis or an incorrect proceeding process (rinse) are some of the possible sources of error. In the next section, it has been made an effort to try to overcome these problems. The synthetic route has been improved, as well as the methodology has been varied.

2.2 SELF-ASSEMBLY OF THIOLS AND SELENOLS ON COPPER SURFACES

2.2.1 INTRODUCTION

After developing the self-assembly system of alkylthiols adsorbed on gold, it was decided to change some elements for the next experiments. The thiol-gold SAM is, with difference, the most studied monolayer system because of its strong interaction and because the resistance of gold to oxidation, among others properties. During the last years, several studies about the use of different kind of substrates have been published. There are several alternatives to gold, such as, silver,[28,29] copper,[30,31] nickel,[32,33] or cobalt,[34,35] which have become interesting platforms for the adsorption of organothiol molecules. In addition, all of them promote the formation of good quality monolayers. Among them, we believe that one of the most interesting and promising surface for further projects is copper. Copper is a ductile metal with higher thermal and electrical conductivity in comparison with gold. Additionally, its lower price makes it a good alternative to substitute gold surfaces. Because of this, copper is very commonly use in the electronic industry.[36] Particularly interesting is their potential application in the design of microelectronic devices and their interconnections. One of the major drawbacks is the rapid oxidation of copper in contact with air. The oxide layer formed on the metal surface can cause an undesired effect in some applications and a chemical or thermal reduction process has been required to carry out its purpose.[37] SAM-surface modification has been suggested in numerous investigations as an alternative to overcome this problem.[31,38,39] Research has not been only focused on adsorption of alkanethiols and other alternatives, such as alkaneselenols derivatives, have been evaluated.[40,41] Since sulphur and selenium belong to the same group on the periodic table, organoselenols were thought to be an alternative for organothiol monolayers. Selenol and diselenide systems are promising candidates for preparation of semiconductor quantum dots or photoinduced electron-transfer systems as the Se-termination provides a better electronic coupling than the sulphur group.[42] Samant *et al*[43] were the firsts to investigate the formation of an organoselenol SAM on gold. In a posterior investigation, Huang[44] concluded that diphenyl diselenide molecules displace benzenethiolate SAM from gold, however diphenyl disulfide molecules do not displace benzeneselenoate SAM. Competitive adsorption experiments showed that free energy of adsorption for diphenyl diselenide was more favourable by 0.7 kcal/mol.

As a consequence, the thiol and the selenol anchoring group in the monolayer formation process have been compared. In this section, alkanethiols and alkaneselenols molecules with a pyrrole terminated group have been employed to form SAMs on a copper substrate. Their behaviour have been studied and characterized and both have been used as nucleation promoters for PPy plasma polymerization.

2.2.2 EXPERIMENTAL PART

2.2.2.1 Chemicals

Substrate for SAM deposition was polycrystalline copper foil 1mm thick, rectangular-shaped (20 x 10 mm) obtained from Goodfellow 99.99% (CU000749). 1,6-Dibromohexane (96%) and 1,12-dibromododecane (98%) were purchased from Aldrich. Thiourea (99%) was obtained from Acros Organics and selenium (powder, 99%) from Riedel-de-Haën. Pyrrole (99%) was purchased from Acros Organics and was purified by distillation. Sodium hydride (60% dispersion in mineral oil), $NaBH_4$ (99%), NaCl (99.5%), NaOH (98%), diethyl ether (99%), formic acid (99%), HCl (37%) and Perchloric acid (70%) were purchased from Acros Organics. DMF (99.8%) was obtained from Lab-Scan, $MgSO_4$ (99.5%) from Aldrich, pentane (95%) and diethyl ether (99%) from Carlo Erba and absolute ethanol from VWR. THF (Acros, 99%) was distilled before use.

2.2.2.2 Synthesis of ω-(N-pyrrolyl)alkanethiol and selenol

The thiol and the selenol target molecules were synthesized via two-step reactions. The first step was the same for both thiol and selenol molecules, and it consisted of the synthesis of the N-Bromoalkylpyrrole. Then, the second step was performed to introduce the appropriate anchoring group in the alkylpyrrole derivative (Scheme 2).

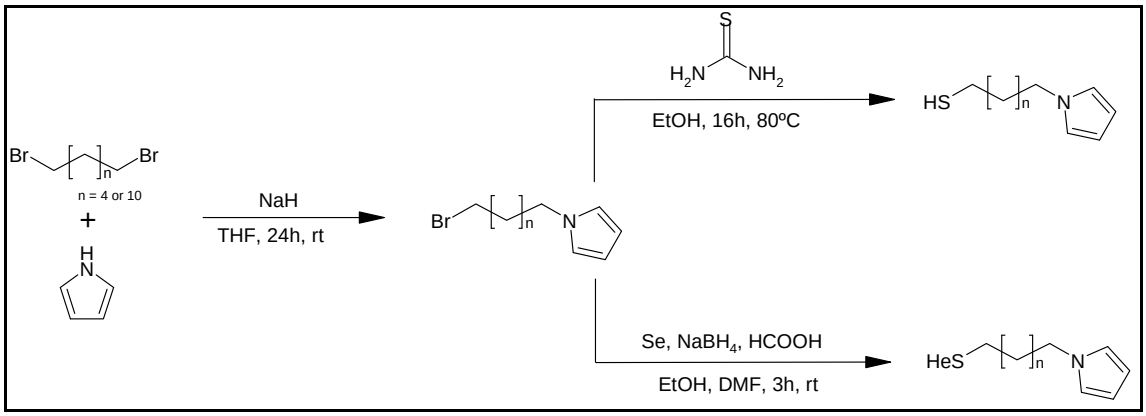

Scheme 2.

Synthesis of N-Bromoalkylpyrrole

In a 250 ml two-necked round bottom flask, sodium hydride (1.8g, 75 mmol) was added to 50 ml of dry THF. At 0ºC, a solution of pyrrole (3.37g, 50 mmol) was added dropwise and the mixture was stirred for 1 h in an inert atmosphere of argon. Afterwards, a solution of dibromoalkane (125 mmol) in 50 ml of dry THF was added dropwise. The mixture was stirred for 3 h at room temperature. Then, 10 ml of water were introduced and the solution was stirred for 30 minutes. After that, the product was extracted with diethyl ether (3 x 30 ml) and the organic phase was washed with 50 ml of HCl 1M and 50 ml of deionized water. Then, the extract was dried ($MgSO_4$) and the solvent removed under reduced pressure. The resulting crude product was purified by chromatography (silica gel (240-400 mesh), pentane/diethyl ether (9/1) (v/v)) to give N-Bromoalkylpyrrole as a yellowish liquid. The N-6-Bromohexylpyrrole yield 63% and the N-12-Bromododecylpyrrole 68%.

^{1}H-NMR ($CDCl_3$, 400 MHz, δ (ppm)): N-6-Bromohexylpyrrole: 1.3-1.5 (m, 4H, C3-C4), 1.7-1.9 (m, 4H, C2 and C5), 3.4 (t, 2H, C6), 3.9 (t, 2H, C1), 6.15 (t, 2H, ArH), 6.66 (t, 2H, ArH). N-12-Bromododecylpyrrole: 1.2-1.9 (m, 20H, C2-C11), 3.4 (t, 2H, C12), 3.85 (t, 2H, C1), 6.1 (t, 2H, ArH), 6.65 (t, 2H, ArH).

Synthesis of ω-(N-pyrrolyl)alkanethiol

The synthesis of 6-(N-pyrrolyl)hexanethiol and 12-(N-pyrrolyl)dodecanethiol has been described previously in 2.1.2.2.

Synthesis of ω-(N-pyrrolyl)alkaneselenol

Sodium borohydride (0.22 g, 6 mmol) and selenium powder (0.22 g, 3 mmol) were introduced into a 50 ml two-necked round bottom flask equipped with a stirring bar and a septum. The flask was kept at room temperature using a water bath, and anhydrous ethanol (1.58 g, 34 mmol) was then added dropwise. The ethanol addition increases the hydrogen evolution and a white-grey solid precipitation. After that, 10 ml of anhydrous DMF were added into the reaction mixture and stirred for 30 minutes. Then, acid formic (0.30 g, 6 mmol) was added dropwise to initiate the hydrogen formation and a white solid formation, and the mixture was stirred for 15 minutes. Then, N-bromoalkylpyrrole (2.5 mmol) was introduced in the mixture and was stirred for 2 hours. The resulting media was quenched with 10 ml of HCl (10%). Afterwards, 50 ml of water was added and the mixture was extracted with diethyl ether (3 x 50 ml), washed with 10% HCl, dried over magnesium sulphate, filtered and the solvent was removed by distilling under reduced pressure.

The 6-(N-pyrrolyl)hexaneselenol (Py6SeH) was obtained in 74%.

^{1}H-NMR ($CDCl_3$, 400 MHz, δ in ppm): -0.68 (t, 1H, SeH), 1.25-1.8 (m, 8H, C2-C5), 2.6 (q, 2H, C1), 3.85 (t, 2H, C6), 6.14 (t, 2H, ArH), 6.64 (t, 2H, ArH).

FT-IR ($CHCl_3$, υ/cm^{-1}): 3098 (arom C-H), 2928 (υ_{as} CH_2), 2854 (υ_s CH_2), 2312 (SeH), 1542-1451 (pyrrole ring), 1359 (C-N).

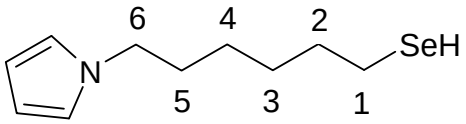

The 12-(N-pyrrolyl)dodecaneselenol (Py12SeH) was obtained in 79%.

^{1}H-NMR ($CDCl_3$, 400 MHz, δ in ppm): -0.68 (t, 1H, SeH), 1.25-1.75 (m, 20H, C2-C11), 2.58 (q, 2H, C1), 3.86 (t, 2H, C12), 6.13 (t, 2H, ArH), 6.64 (t, 2H, ArH).

FT-IR ($CHCl_3$, υ/cm^{-1}): 3100 (arom C-H), 2923 (υ_{as} CH_2), 2851 (υ_s CH_2), 2311 (SeH), 1540-1464 (pyrrole ring), 1366 (C-N).

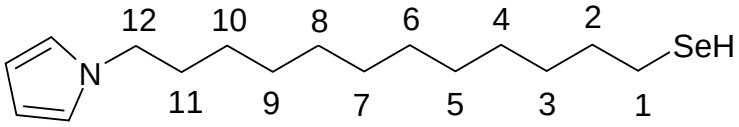

2.2.2.3 Substrate preparation

Polishing

Copper was prepared by mechanical polishing to achieve an average surface roughness of 10 nm. Polishing was performed in a BUEHLER, PHOENIX 4000 equipment, following the procedure described below.

First, substrates were dipped into acetone and sonicated for 30 minutes.

Dry samples were first polished with a 1200 silicon carbide paper grid at 10 N force and 300 rpm for 2 minutes. After that, samples were washed copiously with water and polishing was repeated again.

After that, the silicon carbide disc was changed by a magnetic nylon disc. A 9 μm diamond paste suspension was charged in the disc with a 20 N force at 300 rpm for 5 minutes. Substrates were washed with Mili-Q water (18.2 MΩ cm) and the polishing was repeated again.

To prevent further particle contamination in the next step, all 9 μm the diamond particles were removed from the disc. To this effect, the disc was washed thoroughly with Mili-Q water at 600 rpm for 20 seconds.

Then, a 3 μm diamond paste suspension was charged in the disc with a 20 N force at 300 rpm for 5 minutes. Substrates were washed with Mili-Q water and the polishing was repeated again.

Finally, the magnetic nylon disc was changed by a cloth disc. A 1 μm diamond paste suspension was charged in the disc with a 20 N force at 300 rpm for 5 minutes. Substrates were washed with Mili-Q water and the polishing was repeated again.

Afterwards, the samples were washed with ethanol followed by sonication in ethanol for 15 minutes. Samples were dried with an argon stream and were kept for further experiments.

Oxide reduction

Before carrying out the self-assembly process, it is necessary to remove the copper oxide layer at the surface. Otherwise, the chemical interaction between the copper and the thiol or the selenol group would not be so effective. Thus, a reduction treatment was performed previous to the self-assembly. Before the reduction treatment, organic contaminants were removed from the surface by an UV-O_3 cleaning (UVO-Cleaner 42-220, Jelight Company Inc) for 15 minutes followed by sonication in absolute ethanol for 15 minutes.

A chronoamperometry procedure was employed to eliminate the copper oxide layer. Chronoamperometry is an electrochemical technique in which the potential of the working electrode is maintained constant and the rate of change of current versus time is measured. The experiment was carried out in an electrochemical cell where the working electrode was the copper substrate, the reference electrode was a saturated calomel electrode (SCE, E^0 = 0.2415 V) and the counter electrode was a platinum electrode. A 0.5 M $HClO_4$ solution was used as electrolyte, which had been previously deoxygenated by bubbling argon for 10 minutes. The potential was fixed at -0.82 V for 10 minutes and a stream of argon was bubbled while the experiment was running.

2.2.2.4 The self-assembly

Once the chronoamperometry experiment was finished the copper substrate was dipped in a 10^{-3} M ω-(N-pyrrolyl)alkanethiol or selenol ethanol solution. It is very important to introduce the copper from the $HClO_4$ solution at the reduction stage to the SAM solution as fast as possible to avoid the surface re-oxidation. To obtain a well-ordered and a defect-free monolayer, copper substrates were immersed into the solution for 16 hours. After that, the sample was rinsed copiously with absolute ethanol followed by two sets of 10 min sonication in absolute ethanol. Due to the intermolecular interaction of pyrrole groups, it is possible to achieve a multilayer instead of a monolayer. Therefore, sonication was done to prevent this undesirable effect. Finally, the modified substrates were stored in argon until further characterization or polymerization.

2.2.2.5 Equipments and methods

NMR spectra were recorded on a JEOL spectrometer (JNM EX-400) at 400 MHz.
Photoelectron spectra of the monolayers were recorded at a 35º take-off angle relative to the substrate surface with a SSX-100 spectrometer using the monochromatized X-ray Al Kα radiation (1486.6 eV). Nominal resolution was measured as full width at half-maximum of 1.0 (core-level spectrum) to 1.5 (survey spectrum). The analysed core-level lines were calibrated against the C 1s binding energy set at 285 eV, characteristic of alkyl moieties. The acquired signals were analysed using mixed Gaussian-Lorentzian curves (80%-20% respectively).

PM-IRRAS data were collected from a Bruker Equinox 55-PMA37 equipped with a liquid-nitrogen-cooled mercury-cadmium-telluride (MCT) detector and a zinc-selenide photoelastic modulator. The infrared light was modulated between s- and p-polarization at a frequency of 50 kHz and an incident light upon the sample surface around 85º. Signals generated from each polarization (R_s and R_p) were detected simultaneously by a lock-in amplifier and used to calculate the differential surface reflectivity ($\Delta R/R$) = ($R_p - R_s$)/ ($R_p + R_s$). The spectra were taken by collecting 640 scans at a spectral resolution of 2 cm^{-1}.

CV and polarization curves electrochemical techniques were used to assess the monolayer quality and its ability to inhibit copper corrosion. The measurements were performed in an EG&G PAR potentiostat model 273A monitored by computer with a PAR research electrochemistry software 250 using a three-electrode electrochemical cell. The working electrode was either an unmodified copper foil or a SAM-modified copper, the auxiliary electrode consisted of a platinum foil and a SCE was used as the reference electrode. A spot cell was used to analyse a well-defined and reproducible area of the sample. The CV experiments were carried out in aerated NaOH (0.1 M) aqueous solution at a sweep rate of 10 $mV \cdot s^{-1}$ and cycled between -1.0 V and 0.4 V Vs SCE. Blocking factor (BF) has been calculated by measuring the area of the copper oxidation peaks for bare copper (charge density of bare copper electrode Q^0) and for copper surface modified by Py6SH, Py12SH, Py6SeH and Py12SeH monolayers (charge density of modified electrode Q) and by applying the following formula BF(%) = 100 x ($Q^0 - Q$)/Q^0. Polarization curves have been obtained from a 0.5 M chloride sodium solution by sweeping the potential from -1 to +1 V Vs SCE at 5mV/s.

2.2.3 SAM CHARACTERIZATION

In this work, a more exhaustive study of the monolayer characterization was performed. Several techniques were used for this purpose. Some of them relay on surface analysis and some others are based on electrochemical experiments. The aim of these experiments was to characterize the chemical composition, the chemical state or the corrosion behaviour, among other properties, to determine the monolayer quality. Mainly, there are two characteristics which are aimed in the monolayer formation. One is a proper bond between the surface and the anchoring group, which is required in order to obtain a stable monolayer. The other is to obtain a high order molecular organization in order to achieve homogeneous properties over the surface.

2.2.3.1 X-ray photoelectron spectroscopy (XPS)

When thiol and selenol molecules are in solution spontaneously react with the copper surface, as it is shown in reactions 4 and 5:

$$R-SH+Cu \rightarrow R-S-Cu+\frac{1}{2}H_2 \quad (4)$$

$$R-SeH+Cu \rightarrow R-Se-Cu+\frac{1}{2}H_2 \quad (5)$$

This technique enables to study the Cu-S or Cu-Se covalent-like bond formation. In this chapter is especially crucial a deep surface analysis. Because copper is a highly oxidizable metal, the substrate preparation plays a very important role. Regarding the electrochemical process, it is absolutely necessary to reduce the copper oxide layer and prevent the formation of a new layer. As it has been commented, the copper oxide avoids the correct assembling between the thiol or selenol anchoring group and the substrate. Therefore, firstly, it should be convenient to carry out a quantitative study of the chemical composition in the monolayer. Figure 17, Figure 18, Figure 19 and Figure 20 show XPS spectra of 6-(N-pyrrolyl)hexanethiol, 12-(N-pyrrolyl)dodecanethiol, 6-(N-pyrrolyl)hexaneselenol and 12-(N-pyrrolyl)dodecaneselenol respectively. Additionally, Figure 21 presents the XPS survey spectrum of the copper substrate in which the self-assembly was carried out.

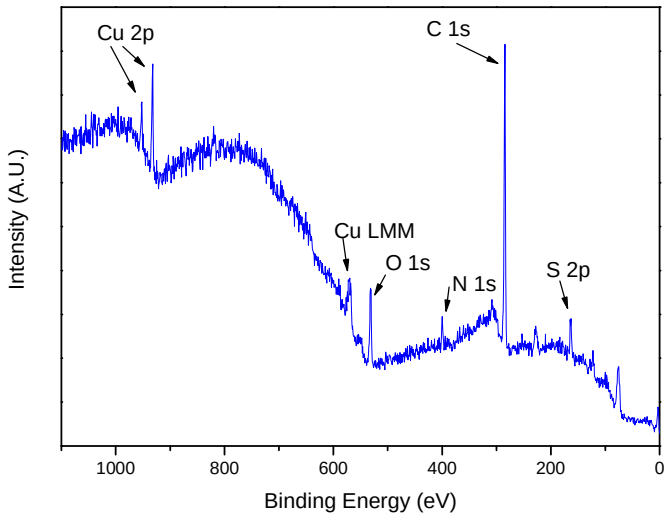

Figure 17. XPS spectrum of a Py6SH monolayer on copper.

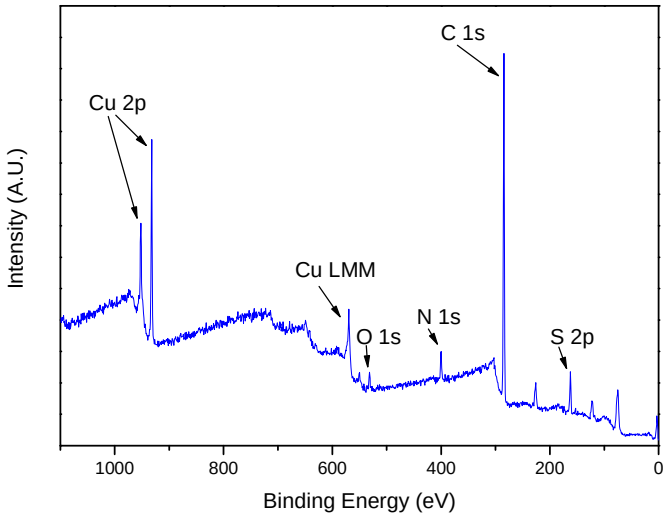

Figure 18. XPS spectrum of a Py12SH monolayer on copper.

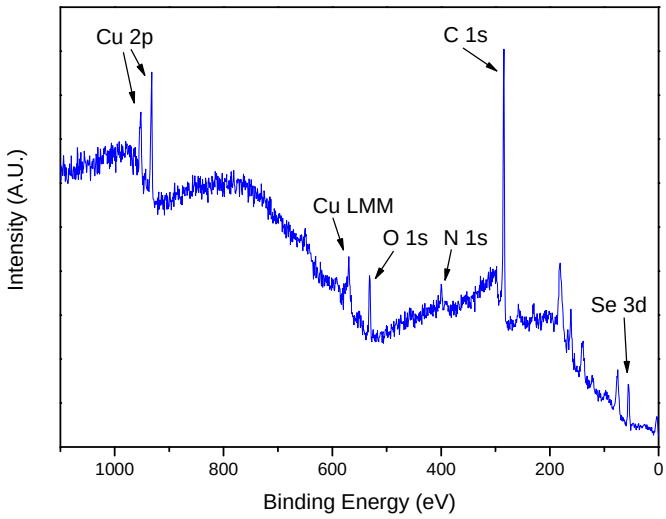

Figure 19. XPS spectrum of a Py6SeH monolayer on copper.

In every spectrum the most important peaks are pointed out: the C 1s at 285 eV, the N 1s at 400 eV, the O 1s at 531 eV, the S 2p at 163 eV or the Se 3d at 55 eV and the Cu 2p, which can be divided into two signals, the $2p_{3/2}$ at 934 eV and the $2p_{1/2}$ at 954 eV. Besides, the Cu LMM peak has been added as it is a feature of the oxidation state of copper. While carbon, nitrogen and sulphur or selenium atoms are found in the molecules assembled onto copper, oxygen-related signals give an idea of the quality of the monolayer. On the other hand, the carbon signal in the copper substrate

corresponds mainly to carbon contaminants and therefore, the oxygen peak corresponds to oxidized species (both carbon and copper). The surface chemical compositions of the different substrates are presented in Table 5.

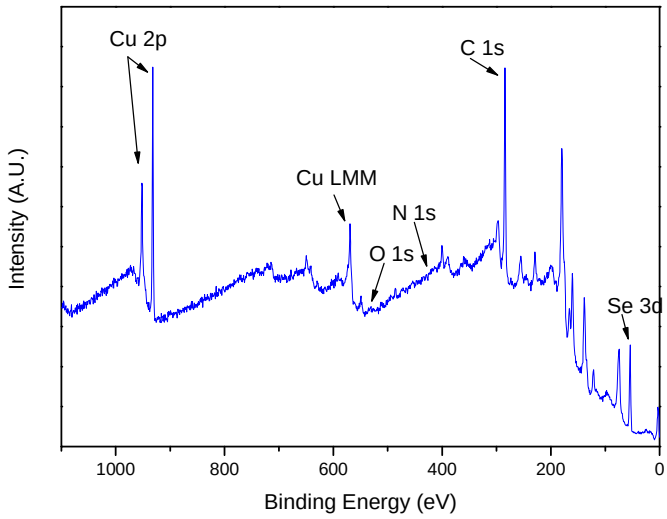

Figure 20. XPS spectrum of a Py12SeH monolayer on copper.

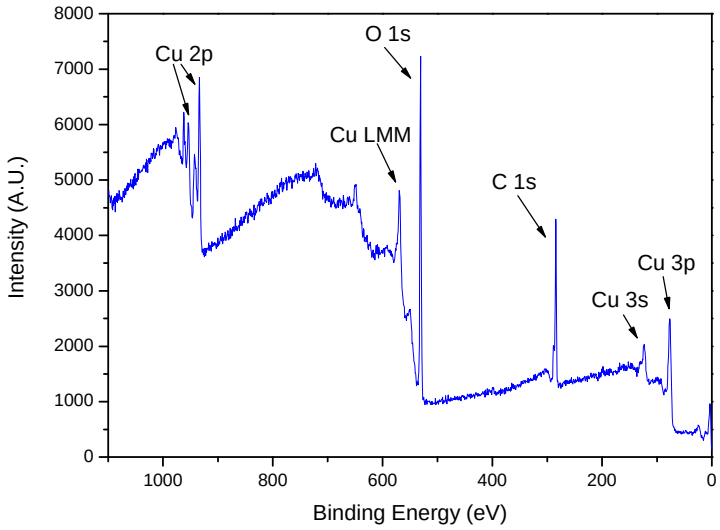

Figure 21. XPS spectrum of copper substrate.

First of all, the amount of oxygen in the sample surface has been studied. It is not worth to compare the oxygen absolute values in Table 5. As a matter of fact, to obtain accurate results it is necessary to compare the ratio of copper atoms to oxygen atoms among all the samples. The Cu/O ratio can be observed in Table 6. As it was expected

the lowest ratio corresponds to the bare copper. If there is no monolayer protecting the surface, the copper oxide covers the entire surface. Turning to the monolayers results, the lowest ratio corresponds to the Py6SH monolayer, followed by the Py6SeH monolayer with values of 0.53 and 1.26 respectively. In contrast, the higher ratios have been found in the Py12SH and Py12SeH, 8.44 and 15.00 respectively.

Table 5. XPS surface composition (%) of the different substrates.

	Cu	Py6SH	Py12SH	Py6SeH	Py12SeH
C (1s)	54.8	80.1	74.9	76.1	66.1
N (1s)	-	4.5	4.7	4.4	4.0
O (1s)	38.2	5.7	1.6	6.1	1.3
S (2p)	-	6.7	5.3	-	-
Se (3d)	-	-	-	5.7	9.1
Cu (2p)	7.0	3.0	13.5	7.7	19.5

Table 6. XPS ratios.

	Cu	Py6SH	Py12SH	Py6SeH	Py12SeH
Cu/O	0.18	0.53	8.44	1.26	15.00
C/N	-	17.80	15.94	17.29	16.52
N/S	-	0.67	0.89	-	-
N/Se	-	-	-	0.77	0.44

A low Cu/O ratio in a monolayer sample means a high amount of the oxide layer. Therefore, it implies that protection against oxidation has not been as efficient as expected. The two lower ratios correspond to monolayers with the shortest alkyl spacing chain (6 methylenes). Numerous studies have attempted to explain how the chain length can affect the monolayer structure.[45-48] It has conclusively been demonstrated that the longer the spacing chain is, the better structured the monolayer is. Consequently, a disordered or not well-packed monolayer can allow oxygen to pass through it and to react with the copper substrate to yield the oxide layer. On the other hand, the monolayers with the longest alkyl spacing chain (12 methylenes) present the highest Cu/O ratios. This result can be explained due to Van der Waal forces. Van der Waal interactions among methylenes help to improve the monolayer quality as it contributes to a better packing. Every methylene contributes 1.5 KJ/mol to the chain-chain interaction energy. Because of this, SAMs with longer alkyl chains are better

packed. As shown in Table 6, there is a significant difference in the Cu/O ratio between the monolayers based on the spacing chain, the relative ratio between SAMs with 6 methylenes (Py6SH and Py6SeH) and SAMs with 12 methylenes (Py12SH and Py12SeH) is in the order of 1 to 15. Furthermore, it can be observed that there is a correlation between the thiol and the selenol monolayer as well. In the selenol monolayers the amount of oxide is lower than in thiol monolayers. The Cu/O ratio for both monolayers is approximately 1 to 2 (1 thiol to 2 selenol). This might suggest that the selenol monolayer is slightly better against the oxide formation. A possible explanation for this effect could rely on the stronger reductive effect of selenol molecules. Another reason may be the undesirable presence of disulfide in the monolayer. In order to obtain a deeper analysis about the chemical composition, a XPS deconvolution analysis was performed.

XPS deconvolution analysis

The XPS deconvolution process consists of an analysis of the desired atoms in a high resolution spectrum. Recording highly resolved spectra in a specific range of energy enables to distinguish the chemical environment of the element. The chemical environment gives information about the oxidation state and about what kind of atom is bonded to. The shape of each peak is composed of the sum of all the chemical state of the atom, giving different binding energy shifts. Thus, the peak fitting is a very powerful tool to investigate the surface chemistry.

The deconvolution analysis was carried out on the anchoring group (both sulphur and selenium) and on the carbon atom. By analyzing the chemical state in the anchoring group, it is possible to determine whether the sulphur and the selenium are covalently attached to the surface or not. The carbon peak gives information about carbon-carbon bonds in the monolayer, carbons linked to the nitrogen atom of the pyrrole moiety and carbon oxidized species among others.

- *S 2p analysis*

The sulphur energy binding ranges from 155 to 175 eV. Figure 22 and Figure 23 show the XPS high resolution spectra of Py6SH and Py12SH, respectively, over the S 2p region. Both spectra are composed of two peaks centered at 162.6 and 163.7 eV. Each peak was fitted with a spin-orbit coupling, with a splitting of 1.18 eV and considering the

area ratio 2 to 1 (S $2p_{3/2}$: S $2p_{1/2}$). Thus, the components lie at 162.6 (S $2p_{3/2}$) and 163.8 eV (S $2p_{1/2}$) for the first peak, and at 163.7 (S $2p_{3/2}$) and 164.9 eV (S $2p_{1/2}$) for the second one. Features with S $2p_{3/2}$ at 162.6 eV can be assigned to copper-bound thiolate (Cu-S-), while those at 163.7 eV can be assigned to unbound thiol (-SH) or disulfide (-S-S-).

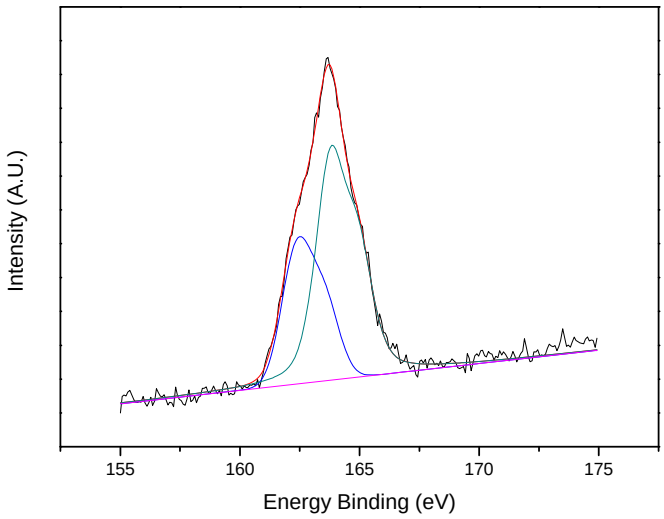

Figure 22. S 2p high resolution XPS spectrum of Py6SH.

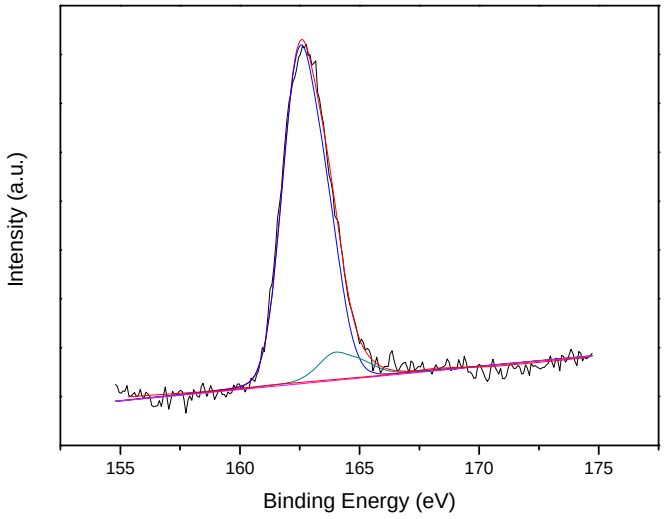

Figure 23. S 2p high resolution XPS spectrum of Py12SH.

- *C 1s analysis*

The carbon energy ranges from 275 to 295 eV. Figure 24 and Figure 25 show the XPS high resolution spectra of Py6SH and Py12SH, respectively, over the C 1s region. The carbon signal has been decomposed into three different peaks according to the different carbon atoms which can be found on the monolayer. The binding energy of 285.9 eV corresponds to carbon atoms bound to nitrogen (C-N). In this study, the nitrogen atom belongs to the pyrrole moiety in the SAM, and thus, the signal reveals the carbons surrounding the nitrogen. The peak at 285 eV can be assigned to the rest of carbon atoms present in the monolayer (C-C). In addition, some spectra show a small signal around 288.0 eV, which is attributed to carbon oxidised species (C_{ox}), such as CO-O-C or CO-OH. The origin of these species can be due to solvent oxidation (ethanol) or even to some atmospheric contaminants.

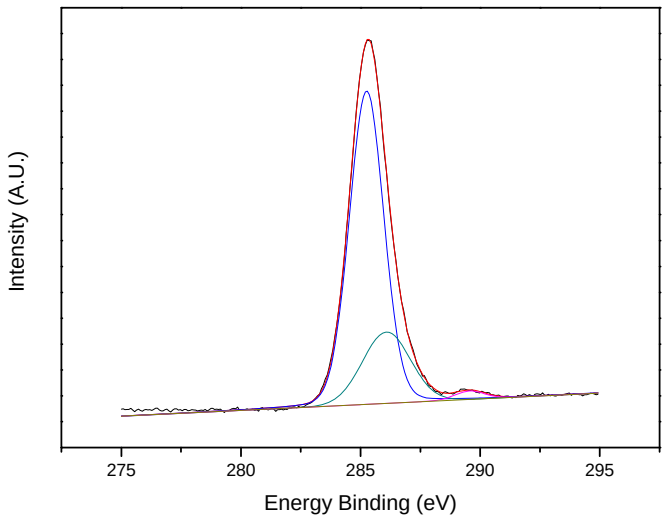

Figure 24. C 1s high resolution XPS spectrum of Py6SH.

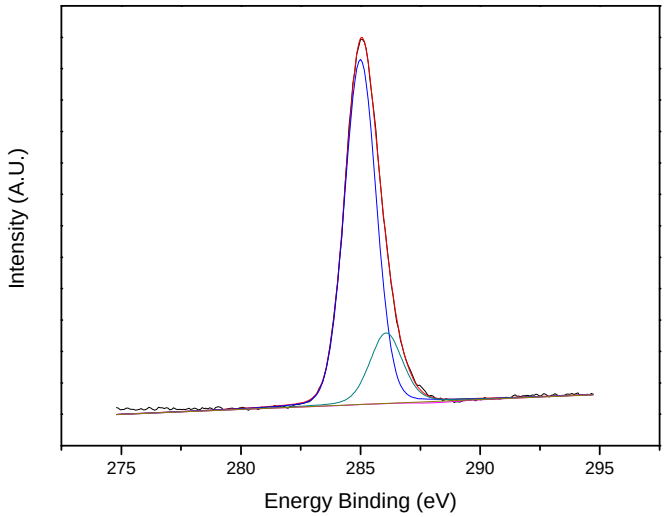

Figure 25. C 1s high resolution XPS spectrum of Py12SH.

XPS has revealed that practically all the Py12SH molecules have been assembled to copper. The ratio between thiolate and unbound thiol or disulfide is 91 to 8. On the other hand, the Py6SH SAM ratio is 37 to 63, which means that the thiol has not been bound so efficiently. It is possible to justify this result because of the fact that Py6SH molecules have been oxidized to yield the disulfide. The 63% which is related to unbound thiol or disulfide moiety can not be distinguished by XPS, because both signals overlap, but it is plausible to assume that the disulfide prevails over the unbound thiol. Moreover, it has been reported previously that disulfide molecules do not assemble properly to oxidized surfaces.[40] Although copper had been reduced to eliminate the copper oxide, some oxygen remaining in the solution can react with it to form the oxide. One of the functions of the monolayers is to protect the surface against corrosion and prevent the oxide layer formation. Nevertheless, at the first stage of the monolayer assembling, oxygen can diffuse more easily through the chain spacer due to the shorter alkyl chain and oxidize the surface. It can be noted that Py6SH SAMs show the highest Cu/O ratio among all the studied samples. Therefore, because of the surface and thiol oxidation the bonding quality achieved by the Py6SH monolayer is not as good as expected. Related to the carbon signal, the ratio between carbon linked to another carbon and carbon linked to nitrogen has been studied. Because of the nitrogen in the pyrrole terminated group, it is possible to distinguish the carbons which form the monolayer. Hence, the theoretical value for the ratio C-C/C-N for the Py6SH and for the Py12SH monolayers are 2.3 and 4.3, and the ratio obtained by the XPS analysis are 2.2 and 4.5 respectively. These results indicate that a high quality

monolayer has been formed, in which, few contaminants or unwanted species are present on the surface.

Table 7. Binding energies and quantitative analysis (%) of the S 2p and C 1s chemical bond corresponding to the Py12SH and Py6SH monolayers.

		Py12SH		Py6SH	
		B.E. (eV)	%	B.E.(eV)	%
S 2p	S-Cu	162.4	91.2%	162.6	36.6%
	S unbound	163.9	8.8%	163.9	63.4%
C 1s	C-C	285	82%	285	75.1%
	C-N	286	18%	285.8	23.2%
	C oxid	288.0	0%	288.6	1.7%

- *Se 3d analysis*

The selenium energy binding ranges from 45 to 65 eV and it shows the XPS high resolution spectra of Py6SeH and Py12SeH, respectively, over the Se 3d region. Both spectra are composed of two peaks centered at 55.0 and 56.8 eV. Each peak was fitted with a spin-orbit coupling, with a splitting of 0.86 eV and considering the area ratio 3 to 2 (Se $3d_{3/2}$: Se $3d_{1/2}$). Thus, the components lie at 55.0 (Se $3d_{3/2}$) and 55.9 eV (Se $3d_{1/2}$) for the first peak, and at 56.8 (Se $3d_{3/2}$) and 57.7 eV (Se $3d_{1/2}$) for the second one. S $2p_{3/2}$ features at 55.0 eV can be assigned to copper-bound selenoate (Cu-Se-), while those at 56.8 eV can be assigned to unbound selenol (-SeH) or diselenide (-Se-Se-).

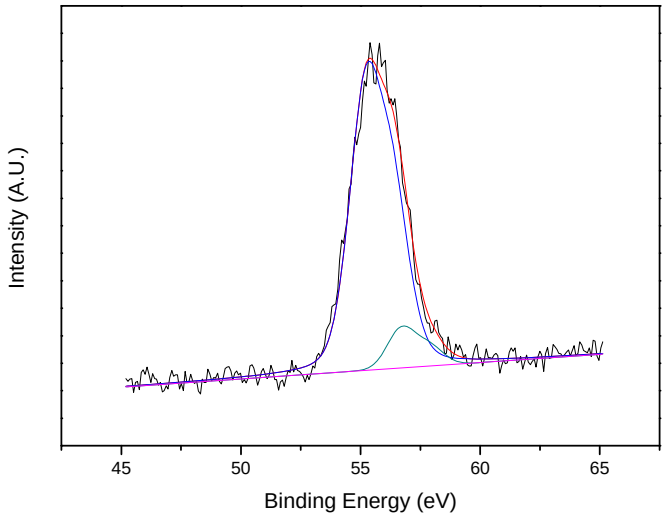

Figure 26. Se 3d high resolution XPS spectrum of Py6SeH.

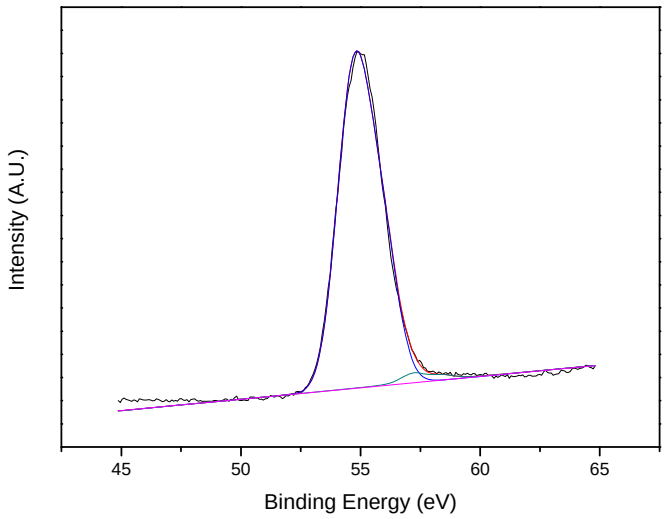

Figure 27. Se 3d high resolution XPS spectrum of Py12SeH.

- *C 1s analysis*

The same study carried out for the thiol monolayers has been done for the selenol monolayers. The carbon signal is analyzed to determine the amount of carbon linked to a carbon atom (C-C), carbon linked to a nitrogen atom (C-N) and the amount of how much carbon oxidized species are presented on the surface. Figure 28 and Figure 29 show the results obtained from the XPS analysis.

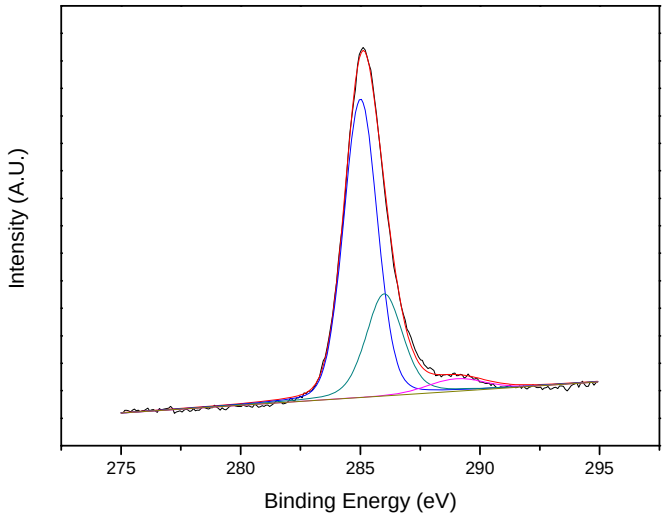

Figure 28. C 1s high resolution XPS spectrum of Py12SeH.

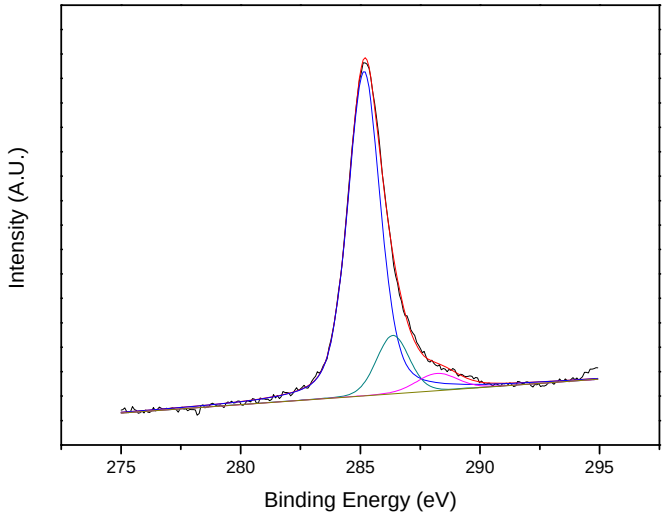

Figure 29. C 1s high resolution XPS spectrum of Py6SeH.

Both selenol monolayers display a high bond efficiency to copper. More than 90% of the molecules are assembled to the substrate. In comparison to the thiol analogues, selenol attached more efficiently to the surface. In this sense, Mekhalif and her group investigated the self-assembling properties of alkanethiol/disulfide and alkaneselenol/diselenide molecules on copper.[40] The selenol group presents a stronger reduction behaviour and because of that, a monolayer can be achieved more easily in oxidized surfaces. At the first stage, a thiol or a selenol can approach to the oxidized

surfaces, and then, it can be oxidized to yield a disulfide or a diselenide and leaving metallic copper at the surface. Next, another thiol or selenol molecule displaces the disulfide or the diselenide and it can be bound to copper. The corresponding reactions are provided in equations 6 and 7, where X can be either S or Se.

$$4RXH + 2CuO \rightarrow 2RXCu + RXXR + 2H_2O \quad (6)$$

$$2RXH + Cu_2O \rightarrow 2RXCu + H_2O \quad (7)$$

The ratio C-C/C-N has been studied for the selenol monolayers as well. The theoretical values for Py6SeH and Py12SeH SAMs are 2.3 and 4.3, and the ones obtained in the experimentally are 2.5 and 4.3 respectively. The observed results fit the expected ratios, which proves the formation of high quality monolayers.

Table 8. Binding energies and quantitative analysis (%) of the Se 3d and C 1s chemical bond corresponding to the Py12SeH and Py6SeH monolayers.

		Py12SeH		Py6SeH	
		B.E. (eV)	%	B.E. (eV)	%
Se 2p	Se-Cu	54.7	97.3%	55.5	90.4%
	Se unbound	57.0	2.7%	56.7	9.6%
C 1s	C-C	285.0	78.3%	285.0	68.5%
	C-N	286	18.2%	286.4	27.1%
	C oxid	287.9	3.5%	288.4	4.4%

Regarding the C 1s deconvolution analysis of thiols assembled on gold, it was necessary to include a peak assigned to an alkoxy group to properly fit the signal. However, in this case, it has not been necessary to include the alkoxy functionality neither for thiol nor selenol for the copper samples deconvolution. The alkoxy peak was justified by the monolayer oxidation and it was related to the detachment of thiolates. For copper samples, the thiolate and selenoate bonds present very high yields, which reveals good quality in the assembling process. Moreover, no evidences of alkoxy groups have been observed in the carbon signal, which could corroborate the hypothesis that monolayer oxidation causes the formation of alkoxy groups.

2.2.3.2 PM-IRRAS

The Polarization Modulation Infrared Reflection-Absorption Spectroscopy (PM-IRRAS) is a technique which enables to study the structure and orientation of very thin films on the surface. Due to polarization modulation of the incident beam at a high frequency, it is possible to eliminate the atmospheric-associated signal (H_2O and CO_2) that may interfere with the sample interpretation. Samples are only sensitive to p-polarization due to the absorption anisotropy on the surface. Hence, difference from the p- and s-polarization lead to the surface characterization. For this reason, PM-IRRAS is being widely employed for SAMs characterization. The monolayer packing depends mainly on the terminal group and the spacer chain. The terminal group, as it has been seen, can vary according to surface requirements. In contrast, the spacer chain is formed usually by methylene units. Several attempts have been made to study the ordering and packing of alkanethiol and alkaneselenol SAMs. Typical peak positions for well-ordered alkanethiol and alkaneselenol monolayers were observed at 2964 (υ_a (CH_3)), 2877 (υ_s (CH_3)), 2918 (υ_a (CH_2)), and 2850 (υ_s (CH_2)) cm^{-1}.[49]

Figure 30 shows the PM-IRRAS spectra of the Py6SH, Py6SeH, Py12SH and Py12SeH monolayers. The absorption bands of asymmetric and symmetric methylene vibrations for Py12SH and Py12SeH monolayers appear at 2926 and 2852 cm^{-1} respectively, and for Py6SH and Py6SeH monolayers at 2927 and 2854 cm^{-1}. Compared to well-ordered monolayers, there has been a shift to higher frequencies in the four monolayers. The higher the frequency is, the worse packed the monolayer is. This shift is due to a loss of ordering attributed to the pyrrole terminated group. A methyl, which is a non-voluminous group, is the terminated group in well-ordered monolayers. As a consequence, chains can get approach. Van der Waals forces rule the interaction among chains and they are the most important factor in the monolayer packing. Thus, in well-ordered monolayers, the interaction among chains reaches the maximum possible because chains are the closest possible. However, pyrrole terminated SAMs are not so well packed, because the pyrrole group is much voluminous than a methyl. In this case, the chains are more separated from each other and Van der Waals interactions decrease. These are the reasons which support the observed absorption shift for the considered monolayers.

Moreover, it can be observed, as expected, that SAMs with the longest alkyl chain present lower absorption frequencies. The relationship between the alkyl chain length and the monolayer ordering has been widely investigated. It has been conclusively

shown that the order of the monolayer increases with increasing the number of methylene units. This phenomenon is attributed to an increase in the number of Van der Waals interactions, which is proportional to the number of methylene units. As it has been explained previously, Van der Waals interactions among chains are one of the most important factors in the formation of ordered monolayers. Thereby, Py12SH and Py12SeH SAMs are better packed than Py6SH and Py6SeH. In addition, no differences have been observed between the thiol and the selenol anchoring group. Thiolate and selenoate bond posses a covalent/ionic nature depending on a stronger pi or sigma character.[50] Covalent radii for S and Se are 1.02 and 1.16 Å, and the ionic radii are 0.37 and 0.50 Å respectively. Since the ionic radii are similar in size, it can be assumed that either thiolate and selenoate bond assemble in a very similar way with the surface and display the same ordering.

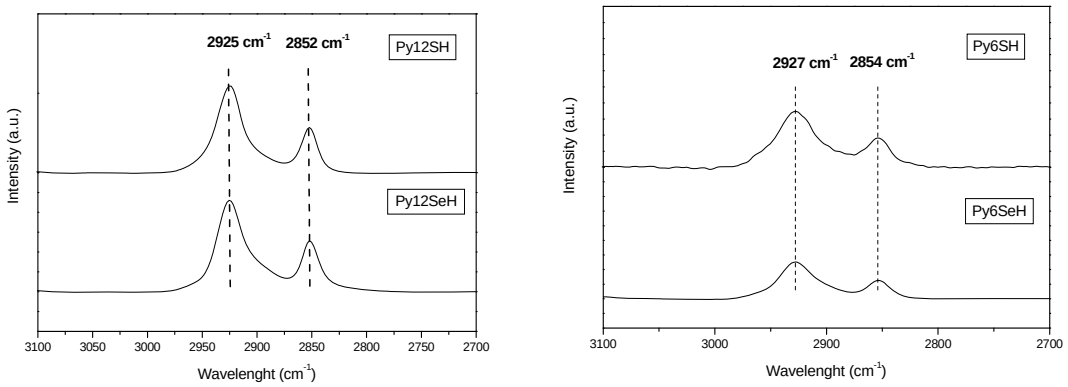

Figure 30. PM-IRRAS spectra of Py6SH, Py6SeH, Py12SH and Py12SeH monolayers.

2.2.3.3 Electrochemical characterization

SAMs are commonly used to prevent undesirable reactions on the surface substrates. The ability of SAMs to block redox reactions lies on the layer efficiency to obtain a dense structure which impedes the mass transport through it. This blocking property is very useful to inhibit corrosion of metals. However, SAMs can present some defects along the layer and these defects can be detected by applying a voltage at the surface and measuring the intensity flow. In order to assess the quality of these SAMs, cyclic voltammetry and polarization curves were recorded and analyzed.

2.2.3.3.1 Cyclic voltammetry

The electrochemical study of the oxidation of copper in aqueous basic media is reported next. Figure 31 displays cyclic voltammograms of bare copper, Py6SH, Py6SeH, Py12SH and Py12SeH. Typical anodic and cathodic peaks are observed in the copper voltammogram. Three oxidation peaks and two reduction peaks can be distinguished.

The corresponding anodic reactions are:

$$2Cu + 2OH^- \rightarrow Cu_2O + H_2O + 2e^- \quad \text{E = -0.40 V} \tag{8}$$

$$Cu_2O + 2OH^- + H_2O \rightarrow 2Cu(OH)_2 + 2e^- \quad \text{E = -0.10 V} \tag{9}$$

$$Cu_2O + 2OH^- \rightarrow 2CuO + H_2O + 2e^- \quad \text{E = 0.10 V} \tag{10}$$

The cathodic reactions are:

$$2CuO + H_2O + 2e^- \rightarrow Cu_2O + 2OH^- \quad \text{E = -0.57 V} \tag{11}$$

$$Cu_2O + H_2O + 2e^- \rightarrow 2Cu + 2OH^- \quad \text{E = -0.93 V} \tag{12}$$

The presence of SAMs should prevent the appearance of oxidation peaks in the anodic scan. However, if there is any defect at the layer, it is possible to observe the electron transfer between the electrode and the media. Thus, some unwanted peaks can appear. A voltammogram of the monolayers have been plotted apart (Figure 32) because in Figure 31 the intensity flow through copper is too high in comparison to the monolayers. Almost no peaks can be detected in the anodic scan which indicates a very good protection against oxidation. Indeed, there is a sharp increase in intensity for Py6SH and Py6SeH monolayer at 0.1 V approximately. This signal is due to molecules desoprtion from the surface. It should be noted that longest monolayers offer higher stability under the chosen conditions as no desorption is observed. Furthermore, to carry out a deeper study of the monolayer protection, the BF has been considered. The BF has been calculated by measuring the area of the copper oxidation peaks for bare copper (charge density of bare copper electrode Q^0) and for copper surface modified by Py6SH, Py12SH, Py6SeH and Py12SeH monolayers (charge density of modified electrode Q) and by applying the following equation:

$$BF(\%) = \frac{Q^0 - Q}{Q^0} \times 100 \quad (13)$$

The BF for Py6SH, Py6SeH, Py12SH and Py12SeH SAMs are 85%, 90%, 95% and 95% respectively. The more percentage of molecules attached to the surface, the more higher the BF is. These results agree with the ones obtained by XPS. If the thiol or the selenol is not properly bound to the copper, the electrons can flow through the working electrode. This electron transfer causes the appearance of oxidation peaks. Nevertheless, Py12SH and Py12SeH have shown a great effectiveness of the surface covering. A BF of 100% has not been reached probably due to the pyrrole moiety. As commented in PM-IRRAS characterization, the monolayer ordering achieved is not the highest that can be obtained due to the bulkiness of pyrrole groups.

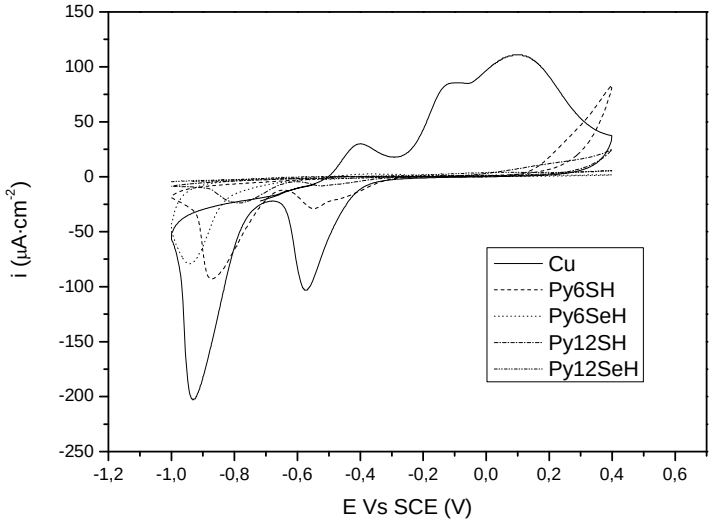

Figure 31. Cyclic voltammogram curves of bare Cu and Py6SH, Py6SeH, Py12SH and Py12SeH monolayers.

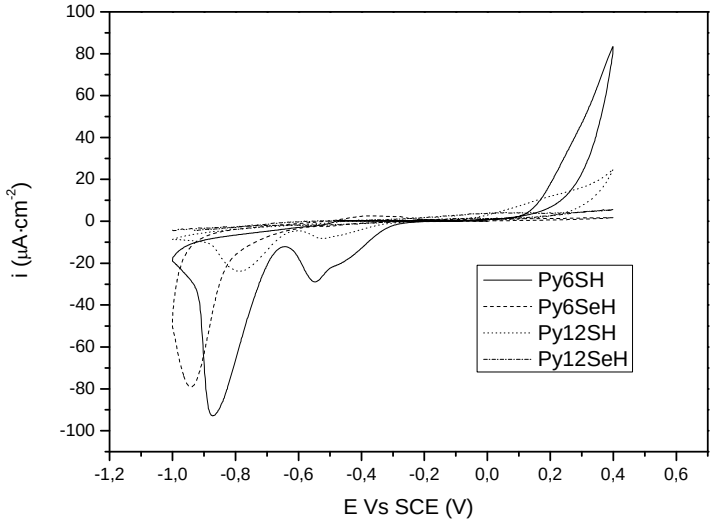

Figure 32. Cyclic voltammogram curves of Py6SH, Py6SeH, Py12SH and Py12SeH monolayers.

2.2.3.3.2 Polarization curves

A polarization curve is another electrochemical tool to evaluate the efficiency of corrosion inhibition. The current (or more often the current density) is plotted against the cell voltage. Typically an alkaline media is used for the experiments: in this case a NaCl solution was used. In addition the chloride anion is known to interfere with the passivation process of copper, resulting in breakdown of the passive film and pitting corrosion.

The copper dissolution in a chloride solution leads to the $CuCl_2^-$ formation, the mechanism is as follows:[51,52]

$$Cu + Cl^- \rightarrow CuCl + e^- \quad (14)$$

$$CuCl + Cl^- \rightarrow CuCl_2^- \quad (15)$$

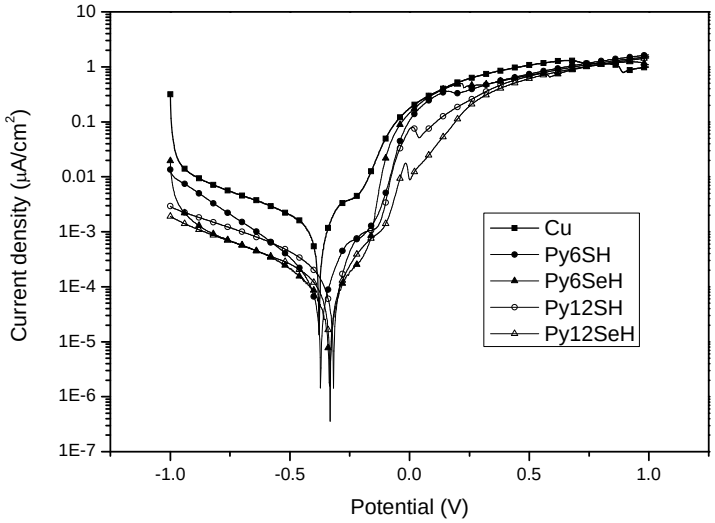

Figure 33. Polarization curves of bare copper, Py6SH, Py6SeH, Py12SH and Py12SeH monolayers.

Polarization curves were obtained from polarizing the samples from -1 V to +1 V, at a scan rate of 5 mV/s.

Figure 33 displays the polarization curves of the different samples. The corrosion potentials and the corrosion current densities were calculated by using Taffel extrapolation method (Table 9). The copper corrosion potential was observed at -373 mV, practically at the same potential than the Py6SH monolayer (-370 mV). In contrast, SAM-modified copper corrosion potentials were shifted towards more anodic potential. The corrosion potentials for Py6SeH, Py12SH and Py12SeH monolayers are quite close to each other and their values are -336, -318 and -332 mV respectively. This shift in the corrosion potential indicates a more efficient protection of the metal surface due to the monolayers protection. The corrosion current densities show an important difference between bare copper and SAMs-modified copper surfaces as well. The measured current densities for the SAMs is about more than 15 times lower than for copper. This result indicates that the monolayers act as an insulator barrier to prevent the copper corrosion. The corrosion current densities for the Py6SeH, Py12SH and Py12SeH monolayers display very similar values (21, 24 and 23 $\mu A/cm^2$), which makes quite difficult to differentiate them. Compared with them, the corrosion current density for Py6SH SAM is slightly higher (32 $\mu A/cm^2$). This difference is owed to the lower quality of the monolayer. Because of the worse ordering and assembling, the current can flow more easily through the monolayer. This result is consistent with those obtained by other characterization techniques and suggests that Py6SH SAM probably presents the worst quality among the four monolayers.

Table 9. Corrosion potentials and corrosion current densities for bare copper, Py6SH, Py6SeH, Py12SH and Py12SeH monolayers.

	Cu	Py6SH	Py6SeH	Py12SH	Py12SeH
Vcorr (mV)	-373	-370	-336	-318	-332
Icorr ($\mu A/cm^2$)	396	32	21	24	23

2.2.3.4 Self-assembling characterization summary

As previously reported, several parameters, such as, surface composition, chemical bonding, ordering and compactness have been investigated in the different monolayers. The most important features are presented in Table 7, Table 8 and Table 10. Almost all the techniques have revealed that Py6S SAMs show the poorest quality. In contrast, Py12SH and Py12SeH have yielded the best quality SAMs. The chain length plays an important role in the monolayer ordering and in their blocking properties. In general, the shortest monolayers are worse structured than the longest ones. Therefore, the difference between 6 and 12 methylene units is enough significant to confer different properties to the monolayers. Furthermore, selenoate bond on copper tends to be more efficient, whereas thiolate bond presents more difficulties, especially in oxidized surfaces. The stronger reduction effect of the selenol group enables it to be attached to the copper despite of the presence of copper oxide.

Due to the high quality of their monolayers, Py12SH and Py12SeH monolayers have been chosen for the next experiments. In order to study the PPy deposition, only one of the two kinds of molecules of each anchoring group has been employed.

Table 10. PM-IRRAS, cyclic voltammetry and polarisation curve results for Py6SH, Py6SeH, Py12SH and Py12SeH monolayers.

	PM-IRRAS		**Cyclic voltammetry**	**Polarization curve**	
	υ_a (cm^{-1})	υ_s (cm^{-1})	BF (%)	V_{corr} (mV)	I_{corr} ($\mu A/cm^2$)
Py6SH	2927	2854	85	-370	32
Py6SeH	2927	2854	90	-336	21
Py12SH	2926	2852	95	-318	24
Py12SeH	2926	2852	95	-332	23

2.3 SELF-ASSEMBLY OF SILANES ON SILICON WAFERS

2.3.1 INTRODUCTION

In the previous assays, a method to deposit PPy on SAM-modified surfaces has been developed. In both cases, the surface was a metal, gold or copper, which had been modified with thiol or selenol molecules. Since sulphur and selenium have similar reactivity, they can be assembled onto the same kind of substrates. For this reason, we decided to change the metal surface for a silicon wafer. The use of SAMs has become particularly helpful for the design of Micro-Electro-Mechanical Systems (MEMS). MEMS are integrated mechanical elements, sensors, actuators and electronics on a common silicon substrate through microfabrication technology. One major limitation in the microfabrication is stinction (static friction), which can result in the failure of the device. The use of monolayers can eliminate the release stinction and reduce the in-use stiction because they act as a passivation layer providing a suitable low energy surface coating. Based on this hypothesis, we wanted to explore the modification of a silicon wafer with a pyrrole-terminated SAM and the posterior plasma polymerization. Most silicon has an oxide layer on the surface and silanes typically form a nicely oriented monolayer on it. Alkyl trichloro or trimethoxy silanes are the most frequent molecules used for the SAM formation on silicon substrates. However, in this investigation a 11-(pyrrol-1-yl-undecyl)dimethylchlorosilane monolayer (Py11Si) has been attached to the silicon wafer.

2.3.2 EXPERIMENTAL PART

2.3.2.1 Chemicals

Potassium (99.95%), 11-bromo-1-undecene (95%), chlorodimethylsilane (98%) and chloroplatinic acid hexahydrate (37.5%) were purchased from Aldrich and were used without further purification. Pyrrole (98%) was purchased from Aldrich and was purified by distillation. DMSO (99.9%), THF (99.9%), toluene (99.8%), diethyl ether (99.7%) and sodium bicarbonate (99.5%) were obtained from Aldrich, CH_2Cl_2 (99.5%), H_2SO_4 (96%), ammonium hydroxide (30%) and H_2O_2 (30%) from Panreac and $MgSO_4$ from Quimivita, all of them were used as received.

2.3.2.2 Synthesis of 11-(pyrrol-1-yl-undecyl)dimethylchlorosilane

The synthesis of the target molecule can be found in literature.[53-55] It consisted of the pyrrole salt formation prepared *in situ* by treatment of potassium with pyrrole followed by reaction with 11-Bromo-1-undecene to yield the 11-(pyrrol-1-yl)undecene. Afterwards, the addition of the silane to the alkene intermediate was achieved using a hexachloroplatinic acid as catalyst (Scheme 3).

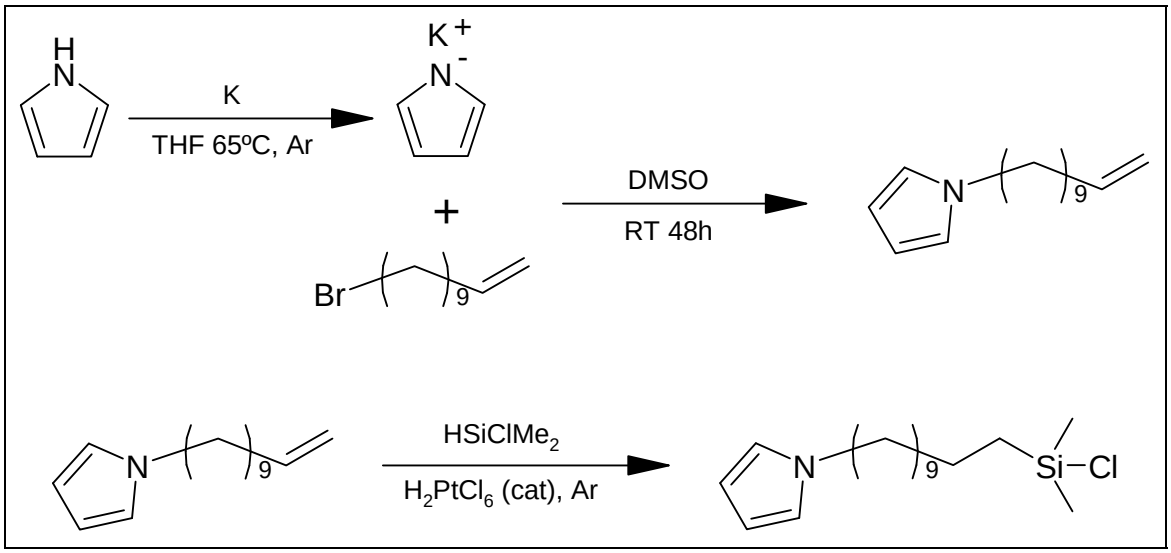

Scheme 3

In a 250 ml round-bottom flask, 30 mmol of potassium freshly cut and 370 mmol of pyrrole were added in 80 ml of dry THF in an inert atmosphere. The mixture was heated and stirred until melting and posterior disappearance of potassium. 20 ml of DMSO were poured. Afterwards, a solution of 60 mmol of 11-Bromo-1-undecene in 100 ml of DMSO was added in a period of 45 minutes. The mixture was stirred at room temperature during 48 hours and then poured into a 50 ml saturated sodium bicarbonate aqueous solution. The product was extracted with diethyl ether (4x25 ml) and dried with anhydrous $MgSO_4$. The organic phase was distilled under reduced pressure to obtain 11-(pyrrol-1-yl)alkene. Further purification was achieved by flash chromatography on silica gel (240-400 mesh) using hexane and dichloromethane (10:1) mixture. The 11-(pyrrol-1-yl)alkene (4.5 mmol) was mixed with 90 mmol of dimethylchlorosilane and a catalytic amount of hexachloroplatinic acid. The mixture was stirred overnight at inert atmosphere. Residual dimethylchlorosilane was removed by distilling under reduced pressure.

11-(pyrrol-1-yl-undecyl)dimethylchlorosilane (Py11Si) was obtained as a dark liquid in 65% yield.

^{1}H-NMR ($CDCl_3$, 300 MHz, δ in ppm): 6.64 (t, 2H, ArH), 6.13 (t, 2H, ArH), 3.86 (t, 2H, C11), 1.75 (m, 2H, C10), 1.35-1.22 (m, 16H, C3-C9), 0.82 (m, 2H, C1), 0.40 (s, 6H, Si-CH3)

FT-IR ($CHCl_3$, υ/cm^{-1}): 3102 (arom C-H), 2923 (υ_{as} CH_2), 2853 (υ_s CH_2), 1540-1464 (pyrrole ring), 1372 (C-N), 840-795 (Si-CH_3), 719 (Si-Cl).

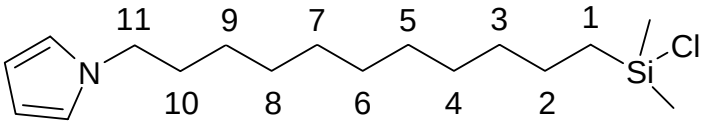

2.3.2.3 Substrate preparation

The self-assembling process requires a hydroxyl terminated group on the surface of the silicon wafer. Despite of the fact that silicon wafers have some hydroxyl groups on the surface, it should be convenient to create more groups to facilitate the assembly. A method for increasing the concentration of hydroxyl groups on the silicon surfaces is described below.

A solution of Milli-Q water, ammonium hydroxide and hydrogen peroxide (vol 5:1:1) was prepared. The silicon wafers were put inside a quartz beaker with the previous solution and the pot was heated up in a water bath. When the temperature reached 80ºC inside the solution, the system was kept 10 minutes at this temperature (important, temperature should not exceed 81ºC). Afterwards, the system was allowed to cool down. At 50ºC the mixture was diluted by adding Milli-Q water. Then it was poured half of the liquid taking care not to expose the substrates to the atmosphere. The substrates must be kept all the time under aqueous solution. The solution was again half diluted in the same way. This step was repeated eight times. When the solution was at room temperature, the silicon wafers were taken off. The substrates were immersed in Milli-Q water twice. After that, the samples were sonicated for 15 minutes in Milli-Q water. The beaker was taken off of the ultrasonic bath and rinsed with Milli-Q water once. Next, the wafers were treated with a mixture of water and chloric acid (36%) in ratio 1:1. The substrates were sonicated again for 15 minutes. Finally, in order to get rid of chloric acid, silicon wafers were rinsed eight times in Milli-Q water as described before.

2.3.2.4 Self Assembly

Formation of the self-assembled monolayer was performed by dipping the silicon wafers previously modified into a 1mM solution of 11-(pyrrol-1-yl-undecyl)dimethylchlorosilane in toluene during 16h. After that, a sonication treatment was done to remove possible physisorption of silane species, then the wafers were blown dry in a stream of nitrogen. Samples were kept under argon atmosphere until further polymerization or characterization.

2.3.2.5 Equipments and methods

NMR spectra were recorded on a Varian Gemini 300 HC apparatus.
FT-IR spectra were collected on a Nicolet Magna 560 FTIR spectrophotometer.
XPS was carried out in a PHI 5500 Multitechnique System (Physical Electronics) with a monochromatic X-ray source (Aluminium Kalfa line of 1486.6 eV energy and 350 W), placed perpendicular to the analyzer axis and calibrated using the 3d5/2 line of Ag. The analyzed area was a circle of 0.8 mm diameter. The XPS spectra were analyzed by the Multipack Version 5.0A software. The binding energy of the core-levels was calibrated against the C 1s binding energy set at 285 eV, an energy characteristic of alkyl moieties. The peaks were analysed using mixed Gaussian-Lorentzian curves (80% of Gaussian character).
The TOF-SIMS analyses were performed using a TOF-SIMS IV mass spectrometer (ION-TOF, Munster, Germany) operated at a pressure of 5 x 10-9 mbar, 18 ns pulses of 25 keV Bi^{3+} (primary ions) were bunched, with an incidence angle of 45º, to form ion packets with a nominal temporal extent of <0.9 ns at a repetition rate of 10 kHz, which produced a target current of 0.2 pA. These primary ion conditions were used to scan a 125x125 μm area of the sample for 30 s.

2.3.3 SAM CHARACTERIZATION

The assembly process consists of a first step, in which the organochlorosilane group is hydrolyzed to form a silanol (the typical reaction for a trichlorosilane is shown in equation 16), which is a more reactive specie. Then, this silanol can get approach and react with a hydroxyl group on the surface to yield the Si-O-Si bond (Equation 17).

$$R - SiCl_3 + 3H_2O \rightarrow R - Si(OH)_3 + 3HCl \quad (16)$$

$$R - Si(OH)_3 + Si - OH \rightarrow R - Si(OH)_2 - O - Si + H_2O \quad (17)$$

The two unreacted hydroxyl group can further react with a neighbour molecule to form intermolecular crosslinking Si-O-Si bonds, to obtain a more compact monolayer.

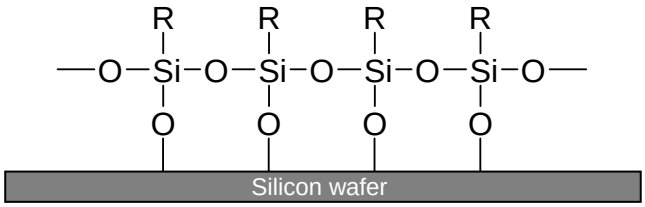

Figure 34. Scheme of a cross-linked silane monolayer.

However, these lateral hydroxyls can react with other free silanol species in solution leading to a more disorder structure (Figure 35). In order to minimize this phenomenon, a dimethylchlorosilane group has been used for the monolayer formation instead of a trichlorosilane (Figure 36). Since the methyl group is more voluminous than a hydroxyl, it is not possible to achieve the same compactness. On the other hand, undesired reactions among close hydroxyls are avoided.

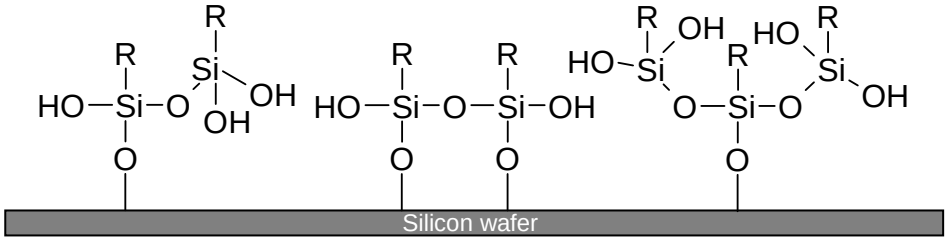

Figure 35. Scheme of a disordered cross-linked silane monolayer.

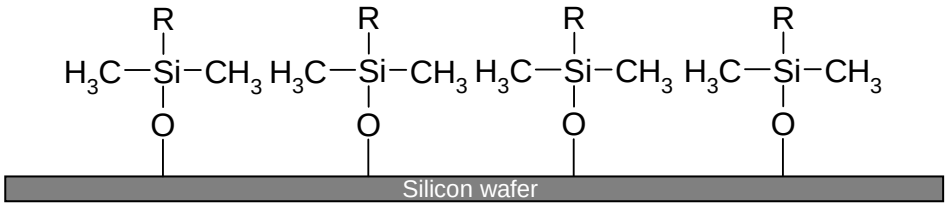

Figure 36. Scheme of a dimethylsilane monolayer.

2.3.3.1 XPS

The survey spectra for the silicon wafer and for the Py11Si SAM are displayed in Figure 37. While the silicon wafer shows only three elements: silicon (2p at 104 eV and 2s at 154eV), carbon (1s at 285 eV) and oxygen (1s, 532 eV), in the SAM-modified silicon wafer appeared another peak corresponding to the nitrogen atom (1s at 400 eV). The new signal can only be due to the pyrrole moiety of the Py11Si SAM.

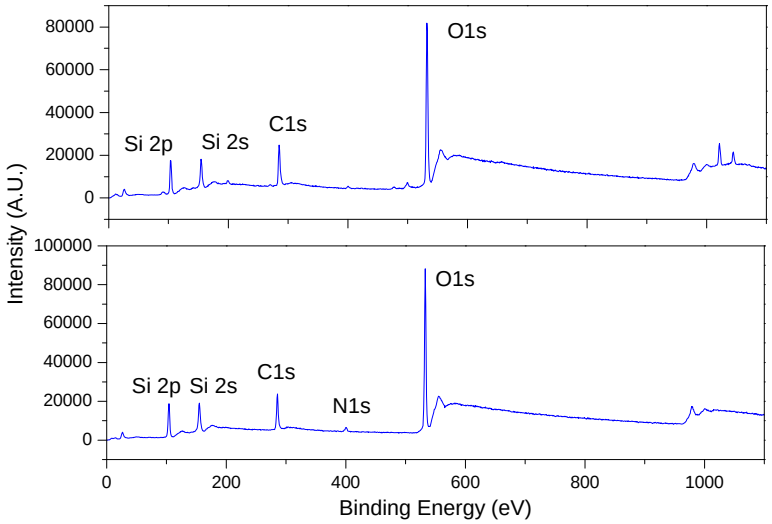

Figure 37. XPS spectrum of a silicon wafer (upper) and of a silicon wafer modified by a Py11Si SAM (lower).

Table 11 compares the surface composition between the silicon wafer and the SAM-modified wafer. For instance, the monolayer formation leads to a C/N ratio decrease, from 37 to 19, due to the nitrogen in the pyrrole moiety. The theoretical value for the C/N ratio in the monolayer should be 17, which is quite close to the obtained. The Si/O ratio for the silicon wafer was 0.48 which practically coincides with the expected value of 0.5, corresponding to the SiO_2 composition. Besides, this ratio increases to 0.56 on the monolayer surface.

Table 11. Surface composition of the silicon wafer and the Py11Si SAM monolayer.

	Si	SAM
C 1s	31.0	26.6
N 1s	0.8	1.4
O 1s	46.2	46.1
Si 2p	22.0	25.8

XPS deconvolution analysis

The deconvolution analysis of C 1s peak in Figure 38 shows the three typical components found in previous SAM analysis: at 288 eV for oxidised carbons (C_{ox}), at 285.9 eV for carbons linked to nitrogen (C-N) and at 285 eV for the rest of carbons which form the monolayer (C-C). The experimental ratio C-C/C-N was found to be 5.0, which is in good agreement with the expected theoretical value, 4.7.

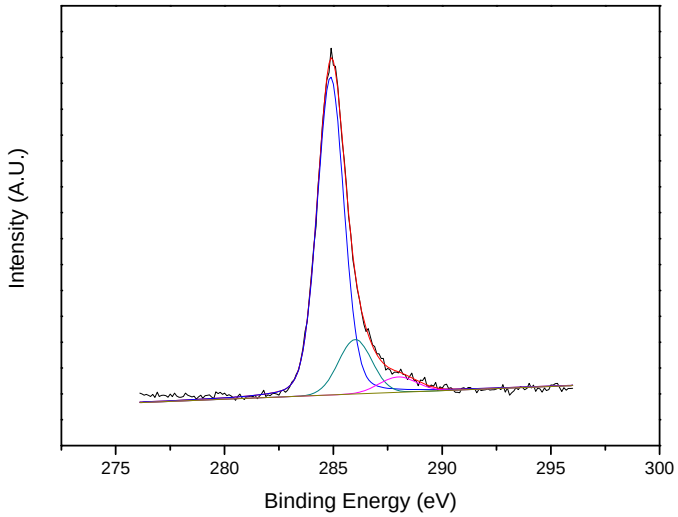

Figure 38. C1s high resolution spectrum of the Py11Si SAM.

Table 12. Binding energies and quantitative analysis (%) of the C 1s chemical bond corresponding to the Py11Si monolayer.

		Py11Si	
		B.E. (eV)	%
C 1s	C-C	285.0	79.1%
	C-N	286.0	15.9%
	C_{ox}	288.0	5.0%

2.3.3.2 TOF-SIMS

TOF-SIMS analysis was performed on the bare substrate and on the SAM-modified silicon wafer because in the XPS analysis was not possible to study accurately the assembly between the silane and the silicon wafer. Since TOF-SIMS allows identifying

the composition and the chemical status near the surface with high sensitivity, a deeper study of the silicon environment was performed. A comparison between the SAM-modified and unmodified silicon wafer surfaces can be observed in Figure 39.

In the positive detection mode spectrum the strongest intensity in the unmodified silicon wafer corresponds to the Si^+ ion (m/z = 28). In contrast, the intensity of this signal significantly decreases in the Py11Si SAM. A previous study of TOF-SIMS performed on alkenes, alkynes and haloalkanes monolayers on silicon reported numerous $SiC_xH_y^+$ fragments and one of the most important feature in all the samples corresponded to the $SiCH_3^+$ ion (m/z = 43), confirming the self-assembly process.[56] This fragment was observed in our SAM-modified surface as well, but the most intense signal was seen at m/z 73. The fragment can be assigned to the $SiC_3H_9^+$ ion, which is a trimethylsilyl derivatives indicator. This ion might form from the fragmentation of the dimetylsilane and the first of the methylene forming the spacer chain, which has been recombined with hydrogen. For this reason, this ion is a good indicator of the monolayer formation. Furthermore, this was supported by the intensities normalised with respect to Si^+ of $SiCH_3^+$ and $SiC_3H_9^+$ (Table 13). Intensity differences between the two surfaces can only be explained by the modification of the silicon wafer with a silane group.

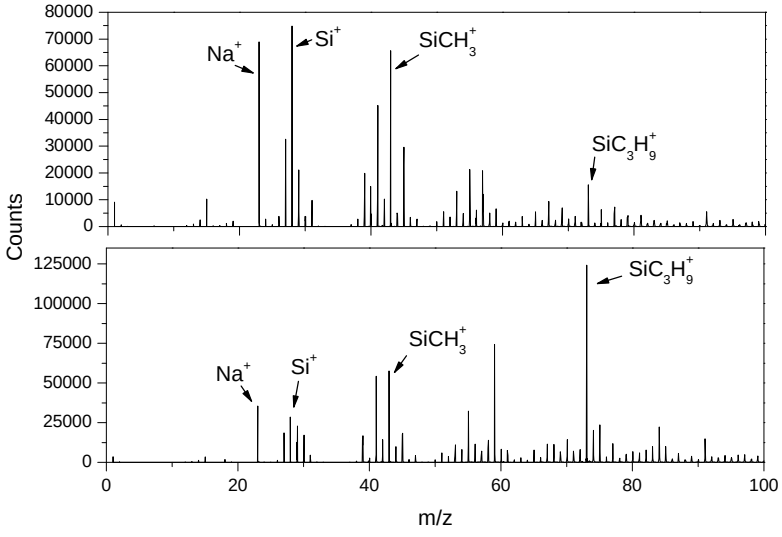

.

Figure 39. Positive TOF-SIMS spectra of the silicon wafer (upper) and the Py11Si SAM (lower) in the mass range m/z 0-100.

Table 13. Relative intensities of $SiCH_3^+$ and $SiC_3H_9^+$ signals on the silicon wafer and the Py11Si SAM.

		Intensity	
Fragment	m/z	Si	SAM
$SiCH_3^+$	43	0.88	2.02
$SiC_3H_9^+$	73	0.21	4.36

In addition, Figure 40 shows the TOF-SIMS negative ion spectra of both surfaces. In the silicon wafer the most intense fragments belong to O^- and OH^- ions (m/z = 16 and 17) and the typical fragment for silicon wafers is assigned to the SiO_2^- anion, at m/z 60. In section 2.1.3.3, some fragments of the N-alkylpyrrole family were found to be characteristics of the self-assembly between thiol and gold surfaces. In contrast to this finding, no evidence of these ions was found on SAM-modified silicon wafers. The only signal that may be due to a pyrrole derivative was seen at m/z 79, corresponding to the $C_5H_5N^-$ ion. Nevertheless, a considerable increase of intensity was found for C_2H^- and CN^- ions (m/z = 25 and 26), which can be attributed to pyrrole fragmentation.[57]

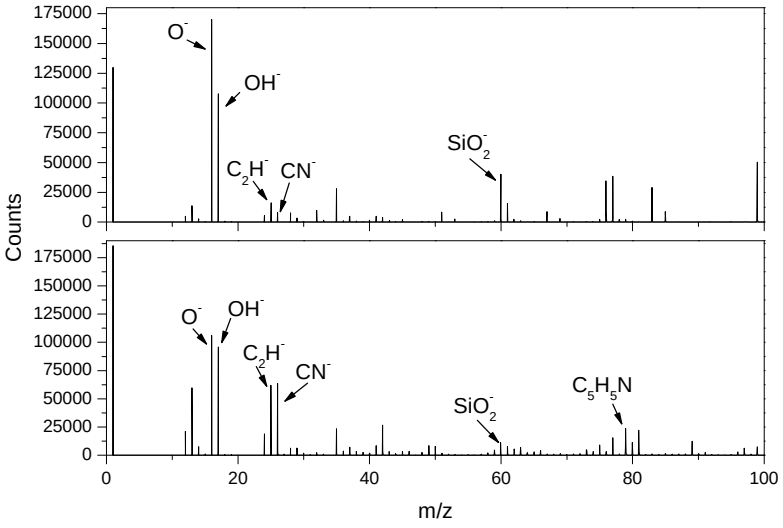

Figure 40. Negative TOF-SIMS spectra of the silicon wafer (upper) and the Py11Si SAM (lower) in the mass range m/z 0-100.

Thus, Table 14 provides C_2H^-, CN^- and $C_5H_5N^-$ ions intensities normalized with respect to SiO_2^- to illustrate the presence of the pyrrole-terminated SAM. The differences found in the three characteristic signals show a different composition in both surfaces. Moreover, the sharp increase for the pyrrole-associated characteristic peaks indicates the presence of pyrrole species due to the SAM formation.

Table 14. Relative intensity of C_2H^-, CN^- and $C_5H_5N^-$ signals on the silicon wafer and the Py11Si SAM.

		Intensity	
Fragment	m/z	Si	SAM
C_2H^-	25	0.38	5.55
CN^-	26	0.18	5.69
C_5H_5N-	79	0.02	1.07

2.4 REFERENCES

1. Nuzzo, R. G.; Allara, D. L. Adsorption of Bifunctional Organic Disulfides on Gold Surfaces. *J. Am. Chem. Soc.* **1983,** *105* (13), 4481-4483.

2. Ulman, A. *Thin Films: Self-Assembled Monolayers of Thiols;* Academic Press: New York, **1998**.

3. Schreiber, F. Structure and growth of self-assembling monolayers. *Prog. Surf. Sci.* **2000,** *65* (5-8), 151-256.

4. Love, J. C.; Estroff, L. A.; Kriebel, J. K.; Nuzzo, R. G.; Whitesides, G. M. Self-assembled monolayers of thiolates on metals as a form of nanotechnology. *Chemical Reviews* **2005,** *105*, 1103-1169.

5. Shukla, R.; Bansal, V.; Chaudhary, M.; Basu, A.; Bhonde, R. R.; Sastry, M. Biocompatibility of gold nanoparticles and their endocytotic fate inside the cellular compartment: A microscopic overview. *Langmuir* **2005,** *21* (23), 10644-10654.

6. Mrksich, M.; Chen, C. S.; Xia, Y. N.; Dike, L. E.; Ingber, D. E.; Whitesides, G. M. Controlling cell attachment on contoured surfaces with self-assembled monolayers of alkanethiolates on gold. *Proc. Natl. Acad. Sci. U. S. A.* **1996,** *93* (20), 10775-10778.

7. Nuzzo, R. G.; Dubois, L. H.; Allara, D. L. Fundamental-Studies of Microscopic Wetting on Organic-Surfaces .1. Formation and Structural Characterization of A Self-Consistent Series of Polyfunctional Organic Monolayers. *J. Am. Chem. Soc.* **1990,** *112* (2), 558-569.

8. Camillone, N.; Chidsey, C. E. D.; Eisenberger, P.; Fenter, P.; Li, J.; Liang, K. S.; Liu, G. Y.; Scoles, G. Structural Defects in Self-Assembled Organic Monolayers Via Combined Atomic-Beam and X-Ray-Diffraction. *J. Chem. Phys.* **1993,** *99* (1), 744-747.

9. Wang, T. X.; Zhang, D. Q.; Xu, W.; Li, S. H.; Zhu, D. B. New approach to the assembly of gold nanoparticles: Formation of stable gold nanoparticle ensemble with chainlike structures by chemical oxidation in solution. *Langmuir* **2002,** *18* (22), 8655-8659.

10. Willicut, R. J.; Mccarley, R. L. Surface-Confined Monomers on Electrode Surfaces - Electrochemical and Microscopic Characterization of Omega-(N-Pyrrolyl)Alkanethiol Self-Assembled Monolayers on Au. *Langmuir* **1995,** *11* (1), 296-301.

11. Wu, C. G.; Chiang, S. C.; Wu, C. H. Formation and electrochemical property of pyrrole-terminated SAMs and the effect of the SAMs on the physicochemical properties of polypyrrole films electrochemically deposited over them. *Langmuir* **2002,** *18* (20), 7473-7481.

12. Castner, D. G.; Hinds, K.; Grainger, D. W. X-ray photoelectron spectroscopy sulfur 2p study of organic thiol and disulfide binding interactions with gold surfaces. *Langmuir* **1996,** *12* (21), 5083-5086.

13. Tour, J. M.; Jones, L.; Pearson, D. L.; Lamba, J. J. S.; Burgin, T. P.; Whitesides, G. M.; Allara, D. L.; Parikh, A. N.; Atre, S. V. Self-Assembled Monolayers and Multilayers of Conjugated Thiols, Alpha,Omega-Dithiols, and Thioacetyl-Containing Adsorbates - Understanding Attachments Between Potential Molecular Wires and Gold Surfaces. *J. Am. Chem. Soc.* **1995,** *117* (37), 9529-9534.

14. Ron, H.; Rubinstein, I. Alkanethiol Monolayers on Preoxidized Gold - Encapsulation of Gold Oxide Under An Organic Monolayer. *Langmuir* **1994,** *10* (12), 4566-4573.

15. Hutchison, J. E.; Postlethwaite, T. A.; Murray, R. W. Molecular Films of Thiol-Derivatized Tetraphenylporphyrins on Gold - Film Formation and Electrocatalytic Dioxygen Reduction. *Langmuir* **1993,** *9* (11), 3277-3283.

16. Tarlov, M. J. Silver Metalization of Octadecanethiol Monolayers Self-Assembled on Gold. *Langmuir* **1992,** *8* (1), 80-89.

17. Laibinis, P. E.; Fox, M. A.; Folkers, J. P.; Whitesides, G. M. Comparisons of Self-Assembled Monolayers on Silver and Gold - Mixed Monolayers Derived from Hs(Ch2)21X and Hs(Ch2)10y (X, y = Ch3, Ch2Oh) Have Similar Properties. *Langmuir* **1991,** *7* (12), 3167-3173.

18. Miller, C.; Cuendet, P.; Gratzel, M. Adsorbed Omega-Hydroxy Thiol Monolayers on Gold Electrodes - Evidence for Electron-Tunneling to Redox Species in Solution. *J. Phys. Chem.* **1991,** *95* (2), 877-886.

19. A.Abdureyim.; K.K.Okudaira; Y.Harada; S.Masuda; M.Aoki; K.Seki; E.Ito; N.Ueno . Characterization of 4-Mercaptohydrocynnamic acid self-assembled film on Au(111) by mens of X-ray photoelectron spectroscopy. *Journal of Electron Spectroscopy and related Phenomena* **2001,** 114-116, 371-374.

20. Castner, C. G.; Hinds, K.; Grainger, D. W. X-ray Photoelectron Spectroscopy Sulfur 2p Study of Organic Thiol and Disulfide Binding Interactions with Gold Surfaces. *Langmuir* **1996**, 12, 5083-5086.

21. Kohli, K.; Taylor, K. K.; Harris, J. J.; Blanchard, G. J. Assembly of Covalently-Coupled Disulfide Multilayers on Gold. *Journal of the American Chemical Society* **1998,** 120, 11962-11968.

22. Schoenfisch, M. H.; Pemberton, J. E. Air Stability of Alkanethiol Self-Assembled Monolayers on Silver and Gold Surfaces. *Journal of the American Chemical Society* **1998,** 120[18], 4502-4513.

23. Tarlov, M. J.; Burgess, D. R. F., Jr.; Gillen, G. UV photopatterning of alkanethiolate monolayers self-assembled on gold and silver. *Journal of the American Chemical Society* **1993,** 115[12], 5305-5306.

24. Willicut, R. J.; Mccarley, R. L. Electrochemical Polymerization of Pyrrole-Containing Self-Assembled Alkanethiol Monolayers on Au. *J. Am. Chem. Soc.* **1994,** *116* (23), 10823-10824.

25. Cabrita, J. F.; Viana, A. S.; Eberle, C.; Montforts, F. P.; Mourato, A.; Abrantes, L. M. Electrooxidation of pyrrole-terminated self-assembled lipoic acid derivatives. *Surf. Sci.* **2009,** *603* (16), 2458-2462.

26. Sayre, C. N.; Collard, D. M. Electrooxidative deposition of polypyrrole and polyaniline on self-assembled monolayer modified electrodes. *Langmuir* **1997,** *13* (4), 714-722.

27. Tarlov, M. J.; Newman, J. G. Static Secondary Ion Mass-Spectrometry of Self-Assembled Alkanethiol Monolayers on Gold. *Langmuir* **1992,** *8* (5), 1398-1405.

28. Widrig, C. A.; Chung, C.; Porter, M. D. The Electrochemical Desorption of N-Alkanethiol Monolayers from Polycrystalline Au and Ag Electrodes. *Journal of Electroanalytical Chemistry* **1991,** *310* (1-2), 335-359.

29. Hutt, D. A.; Cooper, E.; Leggett, G. J. Structure and mechanism of photooxidation of self-assembled monolayers of alkylthiols on silver studied by XPS and static SIMS. *Journal of Physical Chemistry B* **1998,** *102* (1), 174-184.

30. Yamamoto, Y.; Nishihara, H.; Aramaki, K. Self-Assembled Layers of Alkanethiols on Copper for Protection Against Corrosion. *J. Electrochem. Soc.* **1993,** *140* (2), 436-443.

31. Laibinis, P. E.; Whitesides, G. M. Self-Assembled Monolayers of N-Alkanethiolates on Copper Are Barrier Films That Protect the Metal Against Oxidation by Air. *J. Am. Chem. Soc.* **1992,** *114* (23), 9022-9028.

32. Mekhalif, Z.; Laffineur, F.; Couturier, N.; Delhalle, J. Elaboration of self-assembled monolayers of n-alkanethiols on nickel polycrystalline substrates: time, concentration, and solvent effects. *Langmuir* **2003,** *19* (3), 637-645.

33. Kane, S. M.; Gland, J. L. Cyclohexanethiol adsorption and reaction on the Ni(100) surface. *Surf. Sci.* **2000,** *468* (1-3), 101-108.

34. Liu, Q.; Ding, J.; Mante, F. K.; Wunder, S. L.; Baran, G. R. The role of surface functional groups in calcium phosphate nucleation on titanium foil: a self-assembled monolayer technique. *Biomaterials* **2002,** *23* (15), 3103-3111.

35. Gawalt, E. S.; Avaltroni, M. J.; Koch, N.; Schwartz, J. Self-assembly and bonding of alkanephosphonic acids on the native oxide surface of titanium. *Langmuir* **2001,** *17* (19), 5736-5738.

36. Murarka, S. P.; Gutmann, R. J.; Kaloyeros, A. E.; Lanford, W. A. Advanced Multilayer Metallization Schemes with Copper As Interconnection Metal. *Thin Solid Films* **1993,** *236* (1-2), 257-266.

37. Kirsch, P. D.; Ekerdt, J. G. Chemical and thermal reduction of thin films of copper (II) oxide and copper (I) oxide. *J. Appl. Phys.* **2001,** *90* (8), 4256-4264.

38. Feng, Y. Q.; Teo, W. K.; Siow, K. S.; Gao, Z. Q.; Tan, K. L.; Hsieh, A. K. Corrosion protection of copper by a self-assembled monolayer of alkanethiol. *J. Electrochem. Soc.* **1997,** *144* (1), 55-64.

39. Jennings, G. K.; Laibinis, P. E. Self-assembled monolayers of alkanethiols on copper provide corrosion resistance in aqueous environments. *Colloids and Surfaces A-Physicochemical and Engineering Aspects* **1996,** *116* (1-2), 105-114.

40. Mekhalif, Z.; Fonder, G.; Auguste, D.; Laffineur, F.; Delhalle, J. Impact of the anchoring groups X (-SH, -S-S-, -SeH and -Se-Se-) of CF3(CF2)(3)(CH2)(11)X molecules self-assembled on oxidised electroplated copper. *Journal of Electroanalytical Chemistry* **2008,** *618* (1-2), 24-32.

41. Fonder, G.; Volcke, C.; Csoka, B.; Delhalle, J.; Mekhalif, Z. Electrochemical and spectroscopic study of C12H25X molecules adsorption on copper sheets, X (-SH, -S-S-, -SeH and -Se-Se-). *Electrochim. Acta* **2010,** *55* (5), 1557-1567.

42. Patrone, L.; Palacin, S.; Charlier, J.; Armand, F.; Bourgoin, J. P.; Tang, H.; Gauthier, S. Evidence of the key role of metal-molecule bonding in metal-molecule-metal transport experiments. *Phys. Rev. Lett.* **2003,** *91* (9).

43. Samant, M. G.; Brown, C. A.; Gordon, J. G. Formation of an ordered self-assembled monolayer of docosaneselenol on gold(111). Structure by surface x-ray diffraction. *Langmuir* **1992,** *8* (6), 1615-1618.

44. Huang, F. K.; Horton, R. C.; Myles, D. C.; Garrell, R. L. Selenolates as alternatives to thiolates for self-assembled monolayers: A SERS study. *Langmuir* **1998,** *14* (17), 4802-4808.

45. Camillone, N.; Leung, T. Y. B.; Schwartz, P.; Eisenberger, P.; Scoles, G. Chain length dependence of the striped phases of alkanethiol monolayers self-assembled on Au(111): An atomic beam diffraction study. *Langmuir* **1996,** *12* (11), 2737-2746.

46. Atre, S. V.; Liedberg, B.; Allara, D. L. Chain-Length Dependence of the Structure and Wetting Properties in Binary Composition Monolayers of Oh-Terminated and Ch3-Terminated Alkanethiolates on Gold. *Langmuir* **1995,** *11* (10), 3882-3893.

47. Fenter, P.; Eisenberger, P.; Liang, K. S. Chain-Length Dependence of the Structures and Phases of Ch3(Ch2)N-1Sh Self-Assembled on Au(111). *Phys. Rev. Lett.* **1993,** *70* (16), 2447-2450.

48. Dubois, L. H.; Zegarski, B. R.; Nuzzo, R. G. Molecular Ordering of Organosulfur Compounds on Au(111) and Au(100) - Adsorption from Solution and in Ultrahigh-Vacuum. *J. Chem. Phys.* **1993,** *98* (1), 678-688.

49. Fonder, G.; Cecchet, F.; Peremans, A.; Thiry, P. A.; Delhalle, J.; Mekhalif, Z. Conformational order of n-dodecanethiol and n-dodecaneselenol monolayers on polycrystalline copper investigated by PM-IRRAS and SFG spectroscopy. *Surf. Sci.* **2009,** *603* (15), 2276-2282.

50. Solomon, E. I.; Gorelsky, S. I.; Dey, A. Metal-thiolate bonds in bioinorganic chemistry. *J. Comput. Chem.* **2006,** *27* (12), 1415-1428.

51. Feng, Y.; Siow, K. S.; Teo, W. K.; Tan, K. L.; Hsieh, A. K. Corrosion mechanisms and products of copper in aqueous solutions at various pH values. *Corrosion* **1997,** *53* (5), 389-398.

52. Liu, X. Y.; Ma, H. Y.; Miao, S.; Zhou, M. Self-assembled monolayers of stearic imidazoline on copper electrodes detected using electrochemical measurements, XPS, molecular simulation and FTIR. *Chin. Sci. Bull.* **2009,** *54* (3), 374-381.

53. Cossement, D.; Pierard, C.; Delhalle, J.; Pireaux, J. J.; Hevesi, L.; Mekhalif, Z. Synthesis of 6-(1 '-pyrrolyl)-n-hexyltrichlorosilane and 6-(1 '-pyrrolyl)-n-hexyltrimethoxysilane: XPS characterization of their monolayers self-assembled on polycrystalline titanium surfaces. *Surf. Interface Anal.* **2001,** *31* (1), 18-22.

54. Pike, A. R.; Patole, S. N.; Murray, N. C.; Ilyas, T.; Connolly, B. A.; Horrocks, B. R.; Houlton, A. Covalent and non-covalent attachment and patterning of polypyrrole at silicon surfaces. *Advanced Materials* **2003,** *15* (3), 254-+.

55. X.Cai *Synthesis and Characterization of Pyrrole based Adhesion Promoter Systems on Oxide Substrates;* Dresden University of technology, **2005**.

56. Lua, Y. Y.; Niederhauser, T. L.; Matheson, R.; Bristol, C.; Mowat, I. A.; Asplund, M. C.; Linford, M. R. Static time-of-flight secondary ion mass spectrometry of monolayers on scribed silicon derived from 1-alkenes, 1-alkynes, and 1-haloalkanes. *Langmuir* **2002,** *18* (12), 4840-4846.

57. Abel, M. L.; Leadley, S. R.; Brown, A. M.; Petitjean, J.; Chehimi, M. M.; Watts, J. F. Tof-Sims Characterization of Electrochemically Synthesized Polypyrrole Films. *Synth. Met.* **1994,** *66* (1), 85-88.